Hornberger TA, Chu WK, Mak YW et al (2006) The role of phospholipase D and phosphatidic acid in the mechanical activation of mTOR signaling in skeletal muscle. Proc Natl Acad Sci USA 103:4741–4746

Hunter RB, Kandarian SC (2004) Disruption of either the Nfkb1 or the Bcl3 gene inhibits skeletal muscle atrophy. J Clin Invest 114:1504–1511

Hunter RB, Stevenson E, Koncarevic A et al (2002) Activation of an alternative NF-kappaB pathway in skeletal muscle during disuse atrophy. FASEB J 16:529–538

Jackman RW, Kandarian SC (2004) The molecular basis of skeletal muscle atrophy. Am J Physiol Cell Physiol 287:C834–C843

Joulia-Ekaza D, Cabello G (2007) The myostatin gene: physiology and pharmacological relevance. Curr Opin Pharmacol 7:310–315

Judge AR, Koncarevic A, Hunter RB, Liou HC, Jackman RW, Kandarian SC (2007) Role for IkappaBalpha, but not c-Rel, in skeletal muscle atrophy. Am J Physiol Cell Physiol 292:C372–C382

Kadi F (2008) Cellular and molecular mechanisms responsible for the action of testosterone on human skeletal muscle. A basis for illegal performance enhancement. Br J Pharmacol 154:522–528

Koh TJ, Tidball JG (1999) Nitric oxide synthase inhibitors reduce sarcomere addition in rat skeletal muscle. J Physiol 519:189–196

Mammucari C, Milan G, Romanello V et al (2007) FoxO3 controls autophagy in skeletal muscle in vivo. Cell Metab 6:458–471

McCarthy JJ, Esser KA (2007) Counterpoint: satellite cell addition is not obligatory for skeletal muscle hypertrophy. J Appl Physiol 103:1100–1102

Mourkioti F, Kratsios P, Luedde T et al (2006) Targeted ablation of IKK2 improves skeletal muscle strength, maintains mass, and promotes regeneration. J Clin Invest 116:2945–2954

Musarò A, McCullagh K, Paul A et al (2001) Localized Igf-1 transgene expression sustains hypertrophy and regeneration in senescent skeletal muscle. Nat Genet 27:195–200

Nader GA, Esser KA (2001) Intracellular signaling specificity in skeletal muscle in response to different modes of exercise. J Appl Physiol 90:1936–1942

O'Connor RS, Pavlath GK (2007) Point: counterpoint: satellite cell addition is/is not obligatory for skeletal muscle hypertrophy. J Appl Physiol 103:1099–1100

Ohanna M, Sobering AK, Lapointe T et al (2005) Atrophy of S6K1(–/–) skeletal muscle cells reveals distinct mTOR effectors for cell cycle and size control. Nat Cell Biol 7:286–294

Powers SK, Kavazis AN, McClung JM (2007) Oxidative stress and disuse muscle atrophy. J Appl Physiol 102:2389–2397

Reiser PJ, Kline WO, Vaghy PL (1997) Induction of neuronal type nitric oxide synthase in skeletal muscle by chronic electrical stimulation in vivo. J Appl Physiol 82:1250–1255

Rennie MJ, Wackerhage H, Spangenburg EE, Booth FW (2004) Control of the size of the human muscle mass. Annu Rev Physiol 66:799–828

Roberts CK, Barnard RJ, Jasman A, Balon TW (1999) Acute exercise increases nitric oxide synthase activity in skeletal muscle. Am J Physiol 277:E390–E394

Rommel C, Bodine SC, Clarke BA, Rossman R et al (2001) Mediation of IGF-1-induced skeletal myotube hypertrophy by PI(3)K/Akt/mTOR and PI(3)K/Akt/GSK3 pathways. Nat Cell Biol 3:1009–1013

Sandri M, Sandri C, Gilbert A et al (2004) FoxO transcription factors induce the atrophy-related ubiquitin ligase atrogin-1 and cause skeletal muscle atrophy. Cell 117:399–412

Sellman JE, DeRuisseau KC, Betters JL et al (2006) In vivo inhibition of nitric oxide synthase impairs upregulation of contractile protein mRNA in overloaded plantaris muscle. J Appl Physiol 100:258–265

Smith LW, Smith JD, Criswell DS (2002) Involvement of nitric oxide synthase in skeletal muscle adaptation to chronic overload. J Appl Physiol 92:2005–2011

Soltow QA, Betters JL, Sellman JE et al (2006) Ibuprofen inhibits skeletal muscle hypertrophy in rats. Med Sci Sports Exerc 38:840–846

Spangenburg EE (2009) Changes in muscle mass with mechanical load: possible cellular mechanisms. Nutr Metab 34:328–335

Spangenburg EE, Booth FW (2006) Leukemia inhibitory factor restores the hypertrophic response to increased loading in the LIF(–/–) mouse. Cytokine 34:125–130

Spangenburg EE, McBride TA (2006) Inhibition of stretch-activated channels during eccentric muscle contraction attenuates p70S6K activation. Appl Physiol 100:129–135

Spangenburg EE, Le Roith D, Ward CW, Bodine SC (2008) A functional insulin-like growth factor receptor is not necessary for load-induced skeletal muscle hypertrophy. J Physiol 586:283–291

Steensberg A, Keller C, Hillig T et al (2007) Nitric oxide production is a proximal signaling event controlling exercise-induced mRNA expression in human skeletal muscle. FASEB J 21:2683–2694

Stitt TN, Drujan D, Clarke BA et al (2004) The IGF-1/PI3K/Akt pathway prevents expression of muscle atrophy-induced ubiquitin ligases by inhibiting FOXO transcription factors. Mol Cell 14:395–403

Suzuki N, Motohashi N, Uezumi A et al (2007) NO production results in suspension-induced muscle atrophy through dislocation of neuronal NOS. J Clin Invest 117:2468–2476

Tatsumi R, Hattori A, Ikeuchi Y et al (2002) Release of hepatocyte growth factor from mechanically stretched skeletal muscle satellite cells and role of pH and nitric oxide. Mol Biol Cell 13:2909–2918

Tatsumi R, Liu X, Pulido A et al (2006) Satellite cell activation in stretched skeletal muscle and the role of nitric oxide and hepatocyte growth factor. Am J Physiol Cell Physiol 290:C1487–C1494

Tidball JG, Lavergne E, Lau KS et al (1998) Mechanical loading regulates NOS expression and activity in developing and adult skeletal muscle. Am J Physiol 275:C260–C266

Tidball JG, Spencer MJ, Wehling M, Lavergne E (1999) Nitric-oxide synthase is a mechanical signal transducer that modulates talin and vinculin expression. J Biol Chem 274:33155–33160

Ventadour S, Attaix D (2006) Mechanisms of skeletal muscle atrophy. Curr Opin Rheumatol 18:631–635

Widrick JJ, Stelzer JE, Shoepe TC, Garner DP (2002) Functional properties of human muscle fibers after short-term resistance exercise training. Am J Physiol Regul Integr Comp Physiol 283:R408–R416

Xia H, Nho RS, Kahm J, Kleidon J, Henke CA (2004) Focal adhesion kinase is upstream of phosphatidylinositol 3-kinase/Akt in regulating fibroblast survival in response to contraction of type I collagen matrices via a beta 1 integrin viability signaling pathway. J Biol Chem 279:33024–33034

Zanchi NE, Lancha AH Jr (2008) Mechanical stimuli of skeletal muscle: implications on mTOR/p70s6k and protein synthesis. Eur J Appl Physiol 102:253–263

Zhao J, Brault JJ, Schild A et al (2007) FoxO3 coordinately activates protein degradation by the autophagic/lysosomal and proteasomal pathways in atrophying muscle cells. Cell Metab 6:472–483

Journal of Neurochemistry

JNC

JOURNAL OF NEUROCHEMISTRY | 2011 | 116 | 1122–1137

doi: 10.1111/j.1471-4159.2010.07167.x

SynArfGEF is a guanine nucleotide exchange factor for Arf6 and localizes preferentially at post-synaptic specializations of inhibitory synapses

Masahiro Fukaya,* Akifumi Kamata,* Yoshinobu Hara,* Hideaki Tamaki,* Osamu Katsumata,* Naoki Ito,†,‡ Shin'ichi Takeda,† Yutaka Hata,§ Tatsuo Suzuki,¶ Masahiko Watanabe,** Robert J. Harvey†† and Hiroyuki Sakagami*

*Department of Anatomy, Kitasato University School of Medicine, Sagamihara, Japan

†Department of Molecular Therapy, National Institute of Neuroscience, National Center of Neurology and Psychiatry, Kodaira, Japan

‡Department of Biological Information, Tokyo Institute of Technology, Nagatsuta, Yokohama, Japan

§Department of Medical Biochemistry, Graduate School of Medicine, Tokyo Medical and Dental University, Bunkyo-ku, Tokyo, Japan

¶Department of Neuroplasticity, Institute on Aging and Adaptation, Shinshu University Graduate School of Medicine, Matsumoto, Japan

**Department of Anatomy, Hokkaido University School of Medicine, Sapporo, Japan

††Department of Pharmacology, The School of Pharmacy, London, UK

Abstract

SynArfGEF, also known as BRAG3 or IQSEC3, is a member of the brefeldin A-resistant Arf-GEF/IQSEC family and was originally identified by screening for mRNA species associated with the post-synaptic density fraction. In this study, we demonstrate that synArfGEF activates Arf6, using Arf pull down and transferrin incorporation assays. Immunohistochemical analysis reveals that synArfGEF is present in somata and dendrites as puncta in close association with inhibitory synapses, whereas immunoelectron microscopic analysis reveals that synArfGEF localizes preferentially at post-synaptic specializations of symmetric synapses. Using yeast two-hybrid and pull down assays, we show that synArfGEF is able to bind utrophin/dystrophin and S-SCAM/MAGI-2 scaffolding proteins that localize at inhibitory synapses. Double immunostaining reveals that synArfGEF co-localizes with dystrophin and S-SCAM in cultured hippocampal neurons and cerebellar cortex, respectively. Both β-dystroglycan and S-SCAM were immunoprecipitated from brain lysates using anti-synArfGEF IgG. Taken together, these findings suggest that synArfGEF functions as a novel regulator of Arf6 at inhibitory synapses and associates with the dystrophin-associated glycoprotein complex and S-SCAM.

Keywords: ADP-ribosylation factor 6, dystrophin, gephyrin, PDZ domain, post-synaptic density.

J. Neurochem. (2011) **116**, 1122–1137.

Chemical synapses are specialized sites of the communication between neurons where information is processed and integrated. Electron microscopy has allowed morphological

Abbreviations used: Arf, ADP ribosylation factor; BRAG, brefeldin A-resistant Arf-GEF; DGC, dystrophin-associated glycoprotein complex; $GABA_AR$, $GABA_A$ receptor; GAP, GTPase-activating protein; GEF, guanine nucleotide exchange factor; GGA1, Golgi-localizing, γ-adaptin ear homology domain, Arf-binding protein 1; GST, glutathione S-transferase; HA, hemagglutinin; IRSP, insulin receptor tyrosine kinase substrate of 53 kDa; MAGI, membrane-associated guanylate kinase with inverted orientation; PDZ, PSD-95/Discs large/Zona occludens 1; PSD, post-synaptic density; SDS, sodium dodecyl sulfate; SDS–PAGE, SDS–polyacrylamide gel electrophoresis; S-SCAM, synaptic scaffolding molecule; synArfGEF(Po), potential synaptic Arf-GEF; VGAT, vesicular γ-aminobutyric acid transporter.

Received November 24, 2010; revised manuscript received December 8, 2010; accepted December 9, 2010.

Address correspondence and reprint requests to Hiroyuki Sakagami, MD, PhD, Department of Anatomy, Kitasato University School of Medicine, Sagamihara, Kanagawa 252-0374, Japan.
E-mail: sakagami@med.kitasato-u.ac.jp

classification of synapses into asymmetric and symmetric types (Gray 1959). Asymmetric synapses, also called Gray's type I synapses, are usually excitatory, use glutamate as a neurotransmitter and are formed on dendritic spines. They feature a prominent electron-dense thickening at the cytoplasmic surface of the post-synaptic membrane called a post-synaptic density (PSD). Intensive proteomic and molecular cloning analyses have identified the molecular components of excitatory PSDs, which consist of glutamate receptors, cell adhesion molecules, scaffolding and adaptor proteins, cytoskeletal proteins, and signaling molecules including regulators of small GTPases, protein kinases and phosphatases (Scannevin and Huganir 2000).

By contrast, symmetric synapses, also called Gray's type II synapses, are usually inhibitory, use either GABA or glycine as neurotransmitters and are mainly formed on dendritic shafts and cell bodies. The PSD at inhibitory synapses is less electron-dense, having a similar size to the active zone on the pre-synaptic membrane. Our understanding of the molecular organization of inhibitory synapses lags behind that of excitatory PSDs, in part because of the difficulty of purification of inhibitory PSDs. Several components such as gephyrin and dystrophin-associated glycoprotein complex (DGC) are found to localize selectively at post-synaptic specializations of inhibitory synapses and are proposed to be essential for the formation and maintenance of inhibitory synapses. Gephyrin is a 93-kDa peripheral membrane protein that was originally co-purified with glycine receptors (Pfeiffer *et al.* 1982). Several lines of evidence indicate that gephyrin is essential for the post-synaptic clustering of glycine receptors (Kirsch *et al.* 1993; Feng *et al.* 1998) and α2- and γ2-subunit containing $GABA_A$ receptors ($GABA_A$Rs) (Essrich *et al.* 1998). Gephyrin functions as synaptic scaffold and regulator of receptor trafficking by interacting with various membrane, signaling, cytoskeletal, and trafficking proteins (Kneussel and Betz 2000; Fritschy *et al.* 2008). Among gephyrin-interacting proteins, collybistin, a guanine nucleotide exchange factor (GEF), was originally considered to govern synaptic gephyrin localization, because collybistin splice variants lacking a *src* homology 3 domain can recruit gephyrin from intracellular aggregates to submembrane clusters in heterologous transfection systems (Kins *et al.* 2000; Harvey *et al.* 2004). However, most isoforms *in vivo* harbor an Src homology 3 domain, which mediates activation of collybistin-mediated gephyrin clustering by neuroligin 2 (Poulopoulos *et al.* 2009). Curiously, studies with collybistin-deficient mice have revealed that collybistin is only essential for gephyrin-dependent clustering of specific subsets of $GABA_A$Rs in the hippocampus and amygdala (Papadopoulos *et al.* 2007), suggesting that other clustering mechanisms must operate at inhibitory synapses. On the other hand, the DGC is a large multiprotein complex that links the extracellular matrix to the cytoskeleton. Several components of the DGC, including α- and β-dystroglycan, dystrophin, and β-dystrobrevin were shown to selectively localize to inhibitory synapses on neuronal somata and dendrites (Knuesel *et al.* 1999; Brunig *et al.* 2002; Levi *et al.* 2002; Grady *et al.* 2006). A study with dystrophin mutant *mdx* mice also demonstrated that a lack of dystrophin reduced the clustering of $GABA_A$R α1 and α2 subunits in the hippocampus and cerebellum (Knuesel *et al.* 1999), suggesting that gephyrin-independent mechanisms also regulate the clustering of $GABA_A$R α1 and α2 subunits.

SynArfGEF(Po), named as a *potential* synaptic guanine nucleotide exchange factor (GEF) for the ADP ribosylation factor (Arf) family of small GTPases, was originally identified by screening for mRNA species associated with the PSD fraction (Inaba *et al.* 2004). SynArfGEF(Po) contains an N-terminal coiled-coil motif, a calmodulin-binding IQ-like motif, central Sec7 domain and pleckstrin homology domain and a C-terminal type I PSD-95/Disc large/Zonula occludens 1 (PDZ)-binding motif (Inaba *et al.* 2004). All Arf-GEFs contain a Sec7 domain, an approximately 200-amino acid protein module that is critical for the catalysis of GDP-GTP exchange on Arf GTPases. SynArfGEF(Po) belongs to the brefeldin A-resistant Arf-GEF (BRAG)/IQSEC subfamily of Arf-GEFs based on the phylogenic classification of Sec7 domains (Cox *et al.* 2004). The Arf family comprises six structurally related members (Arf1-6) that play an essential role in membrane trafficking and cytoskeletal rearrangements (D'Souza-Schorey and Chavrier 2006). Among six Arf members, Arf6 is the most divergent in terms of structure, localizes at plasma membrane and endosomes, and regulates recycling of the plasma membrane and peripheral actin cytoskeleton. In neurons, Arf6 is implicated in the formation and maintenance of dendritic spines (Choi *et al.* 2006), the branching of axons and dendrites (Hernandez-Deviez *et al.* 2002, 2004), exocytosis and endocytosis of synaptic vesicles (Vitale *et al.* 2002; Krauss *et al.* 2003) and receptor internalization (Delaney *et al.* 2002; Krauss *et al.* 2003; Claing 2004; Houndolo *et al.* 2005). SynArfGEF(Po) mRNA is expressed widely in the rat brain and localized at dendrites as well as cell bodies, suggesting activity-dependent local translation (Inaba *et al.* 2004). Although synArfGEF(Po) protein shows a punctate appearance in cell bodies and dendrites of cultured neurons, its subcellular localization has not been characterized in detail to date.

To obtain a better understanding of the functional significance of synArfGEF(Po), we first demonstrated its ability to activate Arf6 and therefore renamed it synArfGEF. Next, we examined the immunohistochemical localization of synArfGEF in the mouse brain. Intriguingly, synArfGEF exhibited somatodendritic localization with a high selectivity for post-synaptic specializations of inhibitory synapses. We further demonstrated the ability of synArfGEF to interact with utrophin/dystrophin and synaptic scaffolding molecule

(S-SCAM) by yeast two-hybrid and pull down assays. These findings indicate that synArfGEF is a novel signaling component at inhibitory post-synaptic sites.

Materials and methods

All animal protocols were approved by the Animal Experimentation and Ethics Committee of the Kitasato University School of Medicine and followed the guidelines of the National Institutes of Health.

Vectors

Mammalian expression vectors for synArfGEF (pCAGGS-FLAG-synArfGEF) and GEP100/BRAG2 (pCAGGS-FLAG-GEP100) were made by amplifying the coding regions of rat synArfGEF and mouse GEP100 using PCR with primers containing *Eco*RI restriction sites (underlined) as follows: sense, 5′-GAATTCATGGAGAGCCTGC TGGAGAACCCGG-3′ and antisense, 5′-GAATTCCTACACCAGG CTCCTGGAGCCACTG-3′ for synArfGEF; sense, 5′-GAATTCAT GCTAGAACGCAAGTATGGGGGAC-3′ and antisense, 5′-GAAT TCTTAGGAGCACAGCACTGGAGGCTG-3′ for GEP100. After subcloning into pGEM-T Easy (Promega, Madison, WI, USA), the cDNA fragments were digested with *Eco*RI and ligated into the same restriction site of pCAGGS-FLAG (Niwa *et al.* 1991; Sakagami *et al.* 2005). A mammalian expression vector for IQ-ArfGEF/BRAG1, pCAGGS-FLAG-IQ-ArfGEF/BRAG1, was described previously (Sakagami *et al.* 2008). The expression vectors for S-SCAM [pCIneoMyc S-SCAM (1–1277), (1–301), (295–578), (423–578)] were described previously (Sumita *et al.* 2007). The expression vectors for C-terminally hemagglutinin (HA) epitope-tagged Arf1 and Arf6 in pcDNA3 (Hosaka *et al.* 1996) were kindly provided by Dr Kazuhisa Nakayama (Kyoto University). The expression vector for C-terminally FLAG-tagged Arf6(Q67L) mutant in pCAGGS-neo (Tanabe *et al.* 2005) was kindly provided by Dr Masanobu Satake (Tohoku University).

For Arf pull down assays, the bacterial expression vector containing the GAT domain of Golgi-localizing, γ-adaptin ear homology domain, Arf-binding protein 1 (GGA1) (Shinotsuka *et al.* 2002) was kindly provided by Dr Kazuhisa Nakayama (Kyoto University).

For pMAL-SXN, a bacterial expression vector that has the same reading frame for the *SalI* cloning site as that of pGEX4T-2 (GE Healthcare, Piscataway, NJ, USA), oligonucleotides containing *SalI*, *XhoI* and *NotI* sites (5′-AATTGTCGACTCGAGCGGCCGCTGCA-3′ and 5′-GCGGCCGCTCGAGTCGAC-3′) were annealed and ligated into the *Eco*RI and *PstI* sites of pMAL-c2 (New England Biolabs, Beverly, MA, USA). To prepare antigens for immunization and affinity purification, the N-terminal region (amino acids 1–293) of rat synArfGEF, the entire coding region of mouse gephyrin, the region between PDZ1 and PDZ2 domain of rat S-SCAM (amino acids 510–570), the region containing 13th and 14th spectrin repeats of mouse utrophin (amino acids 1761–2101) were amplified by PCR with the following primers containing a *SalI* site (underlined) in sense primers and a stop codon (small letters) in antisense primers: 5′-GTCGACCATGGAGAGCCTGCTGGAGAACCCGG-3′ and 5′-ctaTAGGTCAAGGGAGAGTTCGTACTC-3′ for synArfGEF; GT CGACCATGGCGACCGAGGGAATGATCCTCAC-3′ and tcaTAG CCGTCCAATGACCATGACATC-3′ for gephyrin; 5′-GTCGAC CTGTCGTGGCTACCCTTTGCCCTTTG and 5′ctaGTGCAA AGAATGAGGTGGCCGGTCTG-3′ for S-SCAM; 5′-GTCGAC GACCCTGCTGGAACTGTTCAAGCTGC-3′ and 5′-ttaCGTTAA CCAGCAGGTGACCTCATCTAGCC-3′ for utrophin. After subcloning into pGEM-T Easy, the cDNA fragments were digested with *SalI* and *NotI* and ligated into the same restriction sites of pGEX4T-2 and pMAL-SXN.

For *in vitro* binding assays, the C-terminal region of rat synArfGEF (amino acids 1122–1194) was amplified by PCR with primers containing a *SalI* site (underlined) (5′-GTCGACCAT GGAGCCCCTGCTGAGCCAGGCTC-3′ and 5′-CTACACCAG GCTCCTGGAGCCACTG-3′). After subcloning into pGEM-T Easy, the cDNA fragment digested with *SalI* and *NotI* was ligated into the same restriction sites of pGEX4T-2. The C-terminal regions of utrophin corresponding to amino acids 2961–3429, 2691–3058, and 2691–2843 and dystrophin corresponding to amino acids 2937–3685 were amplified by PCR using the primer combinations listed in Table S1 and ligated into pGEM-T Easy. The inserts were digested with *SalI* and *NotI* and ligated into the same sites of pGEX4T-2.

To construct bait vectors for yeast two-hybrid assays, the C-terminal regions of synArfGEF shown in Fig. 7b were amplified by PCR with primer combinations listed in Table S1 and rat synArfGEF cDNA as a template. After ligation into pGEM-T Easy, the inserts were ligated into *SalI* and *NotI* sites of pDBLeu (Invitrogen Corp., Carlsbad, CA, USA) downstream and in frame with the GAL4 DNA binding domain. For pDBLeu-syn-ArfGEF(PPPPY → PPAPA), mutations were introduced in a PY motif at the C-terminus of synArfGEF using the PrimeSTAR mutation basal kit (Takara, Tokyo, Japan) with pDBLeu-syn-ArfGEF(1122–1194) and mutagenesis oligonucleotides (sense, 5′-CCCCAGCCCCAGCCAACCACCCTCACCAGTT-3′; antisense, 5′-GTGGTTGGCTGGGGCTGGGGGTGGGGGCAGTGG-3′). To construct prey vectors encoding truncated mutants of utrophin and dystrophin as shown in Fig 6a, PCR was carried out with the primer combinations listed in Table S1. After ligation into pGEM-T Easy, the inserts digested with *SalI* and *NotI* were ligated into the same sites of pPC86. All inserts created in this study were confirmed by Sanger DNA sequencing.

Arf Pull down assay

The GEF activity of synArfGEF was examined by Arf pull down assays with GGA1 as described previously (Takatsu *et al.* 2002; Sakagami *et al.* 2006). COS-7 cells were transfected with pcDNA3-Arf1-HA or pcDNA3-Arf6-HA in the presence or absence of pCAGGS-FLAG-synArfGEF using Lipofectamine 2000 (Invitrogen). Cells were lysed in a buffer containing 50 mM Tris–HCl (pH 7.5), 100 mM NaCl, 2 mM $MgCl_2$, 0.1% sodium dodecyl sulfate (SDS), 0.5% sodium deoxycholate, 1% Triton X-100, 10% glycerol and a cocktail of protease inhibitors (Complete Mini™, Roche, Mannheim, Germany). After centrifugation, the supernatants were incubated with 40 μg of glutathione S-transferase (GST)-GGA1 fusion protein immobilized on glutathione-Sepharose 4B (GE Healthcare) for 1 h at 4°C. The precipitates and lysates were separated by SDS–polyacrylamide gel electrophoresis (SDS–PAGE) and subjected to Western blot analysis with anti-HA (Clontech Laboratories, Palo Alto, CA, USA) or anti-FLAG antibodies (M2, Sigma-Aldrich, Inc., St Louis, MO, USA). Immunoreactive bands

were visualized using a chemiluminescent reagent (ECL-PLUS Western blotting detection kit, GE Healthcare) and X-ray films. ImageJ (NIH) was used to measure the densities of immunoreactive bands and statistical analysis was performed using Student's *t*-test.

Transferrin incorporation

HeLa cells were transfected with pcDNA3-Arf6(Q67L)-FLAG or pCAGGS-FLAG-synArfGEF plus pcDNA3-Arf6-HA using Lipofectamine 2000. One day after transfection, cells were serum-starved for 3 h and incubated with Alexa488-conjugated transferrin (25 μg/mL) for 20 min at 37°C. The cells were then fixed with 4% paraformaldehyde and immunostained with anti-FLAG IgG. Fluorescent images and intensities were acquired using a confocal microscope (TCS SP2 AOBS, Leica Microsystems, Wetzlar, Germany). The fluorescent intensities of cytoplasmic transferrin in transfected cells were statistically compared with those in non-transfected cells observed in the same fields using Scheffe's test. Three independent experiments were performed.

Antibodies

The fusion proteins of GST and maltose-binding protein to synArfGEF, gephyrin, S-SCAM, or utrophin were expressed in *Escherichia coli* BL21 (DE3) (Stratagene) in the presence of 1 mM isopropyl β D-thiogalactopyranoside and purified with glutathione-Sepharose 4B and amylose-resin (New England Biolabs), respectively. These GST fusion proteins were then used to immunize rabbits and guinea pigs. The antibodies were affinity-purified with CNBr-activated Sepharose (GE Healthcare) coupled with respective maltose-binding protein fusion proteins. The specificity of antibodies for gephyrin, S-SCAM, utrophin was characterized by Western blot analysis (Figure S1).

Western blot analysis

Mouse brains and COS-7 cells transfected with pCAGGS-FLAG-synArfGEF, pCAGGS-FLAG-IQ-ArfGEF/BRAG1 or pCAGGS-FLAG-GEP100 were homogenized with a buffer containing 125 mM Tris–HCl, pH 6.8, 4% SDS, 20% glycerol, 1% sodium deoxycholate, 10% β-mercaptoethanol and a cocktail of protease inhibitors (Complete Mini™, Roche) and boiled for 5 min. After centrifugation, the lysates were separated by SDS–PAGE and transferred onto polyvinyl difluoride membranes (PVDF-PLUS, Micron Separations Inc., Westborough, MA, USA). The membranes were incubated with antibodies against synArfGEF (0.5 μg/mL) or FLAG (M2, Sigma-Aldrich, 0.5 μg/mL) and subsequently with peroxidase-conjugated secondary antibodies. Immunoreactive bands were visualized using a chemiluminescent reagent (ECL-PLUS Western blotting detection kit, GE Healthcare).

Immunostaining

To confirm the specificity of antibodies, COS-7 cells were plated onto 35-mm dishes at the density of 2×10^5 per dish and transfected with pCAGGS-FLAG-synArfGEF, pCAGGS-FLAG-IQ-ArfGEF/BRAG1 or pCAGGS-FLAG-GEP100 using Lipofectamine 2000 (Invitrogen). Twenty-four hours after transfection, cell were fixed with 4% paraformaldehyde and subjected to double immunostaining with antibodies against synArfGEF and FLAG epitope.

Under deep anesthesia with diethyl ether, C57BL/6N male mice at postnatal 10–12 weeks transcardially fixed with 4% paraformaldehyde plus 0.2% picric acid in 0.1 M phosphate buffer (pH 7.4). Brains were further immersed with the same fixative overnight, cryoprotected in 30% sucrose, and sliced at a thickness of 30 μm with a cryostat. Hippocampal cultures were prepared from 18-day-old rat embryos at the plating density of 0.6×10^6 per 35-mm dish as described previously (Sakagami *et al.* 2005). At 22 days *in vitro*, plates were fixed with 2% paraformaldehyde for 5 min.

For immunoperoxidase staining, brain sections were solubilized in 0.3% Triton X-100 for 30 min, blocked with 5% normal goat serum for 30 min, and incubated with anti-synArfGEF IgG (1 μg/mL) overnight. After washing extensively with phosphate-buffered saline, they were subsequently incubated with peroxidase-conjugated anti-rabbit IgG (Histofine Simple Stain MAX PO (R) kit, Nichirei, Tokyo, Japan) for 1 h at 23°C. Immunoreactions were visualized with 3,3′-diaminobenzidine tetrahydrochloride chromogenic substrate (Liquid DAB and Substrate Chromogen System, K3468; DAKO, Tokyo, Japan). The pre-embedding silver-enhancement immunogold method was described previously (Sakagami *et al.* 2008). Briefly, after incubation with the primary antibody, the sections were incubated with nanogold-conjugated anti-rabbit IgG (1 : 100, Nanoprobes Inc., Yaphank, NY, USA), washed with phosphate-buffered saline, and fixed with glutaraldehyde for 10 min. The gold labeling was intensified for 3–5 min under a safety red light using a HQ Silver Enhancement kit (Nanoprobe Inc.) according to the manufacturer's instructions. The sections were treated with 1% osmium tetroxide and 2% uranyl acetate, dehydrated with ethanol and embedded in epoxy resin. Ultrathin sections were examined with a JEM-1230 electron microscope (JEOL Ltd., Tokyo, Japan).

For immunofluorescent staining, samples were incubated with the combination of rabbit or guinea pig polyclonal anti-synArfGEF IgG with guinea pig anti-gephyrin IgG, guinea pig anti-PSD-95 IgG (Fukaya and Watanabe 2000), rabbit anti-IQ-ArfGEF/BRAG1 (Sakagami *et al.* 2008), rabbit $GABA_AR$ α1 subunit IgG (Alamone Labs, Jerusalem, Israel), anti rabbit anti-vesicular GABA transporter (VGAT) (Fukudome *et al.* 2004), guinea pig anti-α-amino-3-hydroxy-5-methyl-4-isoxazolepropionate-type glutamate receptor GluA2 subunit IgG (Yamazaki *et al.* 2010), guinea pig anti-S-SCAM IgG, mouse monoclonal anti-glycine receptor α1 subunit IgG (clone mAb4a, Synaptic Systems, Gottingen, Germany) or anti-dystrophin IgG (MANDRA-1, Sigma). Immunoreactions were visualized with the appropriate combination of the following secondary antibodies: Alexa488-conjugated anti-rabbit IgG, Alexa488- or Alexa594-conjugated anti-guinea pig IgG, and Alexa594- or Alexa647-conjugated anti-mouse IgG (Molecular Probes, Inc., Eugene, OR, USA). Nuclei were counter-stained with 4′,6-diamidino-2-phenylindole dihydrochloride. Immunofluorescent images were taken with a confocal microscope (LSM 710, Carl Zeiss, Oberkochen, Germany) using ×20 and ×63 plan-apochromat objective lens. The brightness and contrast of the final images were adjusted using Photoshop CS4 software (Adobe Systems, San Jose, CA, USA). In control experiments, the primary antibody was pre-incubated with the antigen (10 μM) before immunostaining.

Yeast two-hybrid assay

Yeast two-hybrid screening was performed as described previously (Sakagami *et al.* 2007, 2008). Briefly, approximately 2×10^6 clones of a mouse brain cDNA library were screened using pDBLeu-

synArfGEF(1122–1194), which encoded the fusion protein of C-terminal 73 amino acids of rat synArfGEF to the GAL4 DNA-binding domain, by the ability to grow on selective medium lacking histidine, leucine and tryptophan supplemented with 10 mM 3-aminotriazole. Positive colonies were further selected by the β-galactosidase assay and uracil prototrophy. Plasmids were subjected to the sequencing analysis. To verify the interaction, the yeast strain MaV203 was co-transformed with the indicated combination of bait pDBLeu and prey pPC86 vectors shown in Figs 6 and 7. The interactions were tested by the β-galactosidase assay and the ability to grow without histidine and uracil.

In vitro binding assay

COS-7 cells were transiently transfected with various plasmid constructs encoding myc-tagged S-SCAM or FLAG-synArfGEF and lysed in the lysis buffer consisting of 50 mM Tris-HCl (pH 7.5), 150 mM NaCl, 1% Nonidet P-40 and a cocktail of protease inhibitors (Complete Mini™, Roche). Lysates were incubated with 15 μg of GST, GST-synArfGEF 1122–1194, GST-utrophin 2691–3429, 2691–3058, 2691–2843, 2937–3685, or GST-dystrophin 2937–3685, immobilized on glutathione-Sepharose 4B for 1 h at 4°C. Afterwards, the beads were washed five times with the lysis buffer containing 150 mM or 300 mM NaCl and the proteins were eluted with SDS sample buffer. The cell lysates and eluates were analyzed by Western blot analysis with anti-myc IgG or anti-FLAG IgG.

For pull down assays from brain extracts, mouse brains were homogenized with 10 volumes of the lysis buffer and centrifuged at 12 000 *g* for 15 min. The supernatant (1 mg) were pre-cleaned with glutathione-Sepharose 4B for 30 min and incubated with 20 μg of GST, GST-utrophin 2691–3429, or GST-dystrophin 2937–3685, which were immobilized on glutathione-Sepharose 4B, for 1 h at 4°C. The precipitates were washed with the lysis buffer containing 150 or 300 mM NaCl and subjected to Western blot analysis with rabbit anti-synArfGEF IgG.

Immunoprecipitation

Immunoprecipitation from brain lysates was performed as described previously (Sakagami *et al.* 2008). Briefly, the mouse brain P2 fraction was solubilized with 1% sodium deoxycholate in 50 mM

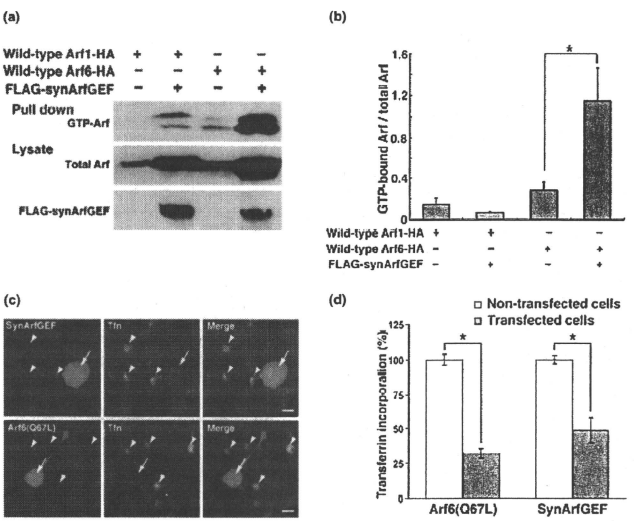

Fig. 1 SynArfGEF activates Arf6. (a) Arf pull down assays. COS-7 cells were transfected with the indicated combination of vectors and were subjected to Arf pull down assays with the GST-GGA1 fusion protein. (b) Quantification of the ratio of GTP-bound Arfs to total Arfs. Note the significant increase in GTP-Arf6 in the presence of FLAG-synArfGEF ($p < 0.01$, Student's *t*-test). Data are represented as mean ± SD from three independent transfection samples. (c) Transferrin incorporation assay. HeLa cells were transfected with FLAG-synArfGEF plus Arf6-HA or Arf6(Q67L)-FLAG. After serum-starvation, cells were incubated with Alexa488-transferrin and subjected to immunostaining. Representative figures show the decreased transferrin incorporation in cells expressing FLAG-synArfGEF and Arf6-HA or Arf6(Q67L)-FLAG (arrows) compared with that in non-transfected cells (arrowheads). Scale bars, 10 μm. (d) Quantification of the fluorescence intensity of intracellular transferrin. Data are represented as mean ± SEM from three independent experiments. Asterisks indicate significant difference of fluorescence intensities between transfected and non-transfected cells ($p < 0.01$, Scheffe's test).

Tris–HCl (pH 9.0) and dialyzed against the binding buffer [0.1% Triton X-100, 50 mM Tris–HCl (pH 7.4)]. After pre-cleaning with Protein G-Sepharose 4B, the soluble supernatant (1 mg) was incubated with 5 μg of anti-synArfGEF IgG or normal rabbit IgG for 1 h at 4°C and with Protein G-sepharose 4B for another 1 h. The beads were washed five times with the binding buffer plus 150 mM NaCl. Proteins were eluted with SDS sample buffer, subjected to SDS–PAGE and immunoblotted with antibodies against S-SCAM (M2441, Sigma) or β-dystroglycan (clone 43DAG1/8D5, Novacastra Laboratories, Newcastle, UK).

Results

SynArfGEF activates Arf6

Two related proteins in the BRAG/IQSEC family of Arf-GEFs, IQ-ArfGEF/BRAG1/IQSEC2 and GEP100/BRAG2/IQSEC1 have previously been shown to activate Arf6 (Someya *et al.* 2001; Sakagami *et al.* 2008). To examine whether synArfGEF/BRAG3/IQSEC3 activates Arf6, we performed Arf pull down assays with a GST-GGA1 fusion protein that is capable of binding GTP-bound Arfs of all classes. COS-7 cells were co-transfected with FLAG-synArfGEF and Arf1-HA or Arf6-HA. Immobilized GST-GGA1 pulled down 4.13-fold more GTP-Arf6-HA from the lysates of COS-7 cells expressing both Arf6-HA and FLAG-synArfGEF than Arf6-HA alone ($p = 0.0092$ by Student's *t*-test, Fig. 1a and b). Co-transfection of Arf1-HA and FLAG-synArfGEF increased both total and GTP-bound Arf1 to a similar extent and did not change the ratio of GTP-Arf1 to total Arf1 (Fig. 1a and b). We further examined the ability of synArfGEF to activate Arf6 *in vivo* using a transferrin incorporation assay. Arf6 has been shown to regulate the endocytosis of transferrin receptor (D'Souza-Schorey *et al.* 1995). If synArfGEF activates Arf6 *in vivo*, transferrin uptake would be affected by over-expressing synArfGEF. We therefore examined the incorporation of transferrin in HeLa cells transfected with FLAG-synArfGEF and Arf6-HA. In non-transfected cells, transferrin accumulated in the perinuclear region (Fig 1c). By contrast, the incorporation of transferrin was reduced by 48.7% in cells transfected with FLAG-synArfGEF and Arf6-HA compared to non-transfected cells (Fig. 1c and d). This reduction was comparable with the reduction (31.9%) observed for cells transfected with the GTP hydrolysis-defective Arf6 mutant, Arf6(Q67L). Taken together, these findings suggest that synArfGEF activates Arf6 *in vivo*.

Preferential localization of synArfGEF at inhibitory synapses

We have previously shown that synArfGEF mRNA is expressed preferentially in the olfactory bulb, cerebral cortex, hippocampus, brainstem nuclei and cerebellar Purkinje cells of the adult rat brain (Inaba *et al.* 2004). In this study, we produced novel anti-synArfGEF antibodies for use in immunohistochemistry. Western blot analysis using the lysates of COS-7 cells transfected with FLAG-tagged BRAG family members showed that both antibodies raised in rabbit and guinea pig detected FLAG-synArfGEF, while they did not cross-react with other BRAG members, FLAG-IQ-ArfGEF/BRAG1 or GEP100 (Fig. 2). In the mouse brain lysate, the antibodies gave two immunoreactive bands of 160 and 130 kDa (Fig. 2), suggesting the existence of two alternatively spliced isoforms as is the case for the other BRAG/IQSEC family members (Dunphy *et al.* 2006; Shoubridge *et al.* 2010). Notably, the electrophoretic mobility of the 160 kDa band was consistent with that of recombinant FLAG-synArfGEF detected using an anti-FLAG antibody (Fig. 2). Further to confirm the specificity, COS-7 cells were transfected with FLAG-tagged BRAG members and subjected to immunostaining. Again, the antibodies specifically detected COS-7 cells transfected with FLAG-synArfGEF without any immunolabeling in non-transfected cells or cells transfected with FLAG-IQ-ArfGEF/BRAG1 or GEP100 (Figure S2). Immunoperoxidase staining of mouse brain sections with rabbit anti-synArfGEF IgG yielded intense labeling in the olfactory bulb, cerebral cortex, hippocampal formation, reticular thalamic nucleus, superior and inferior colliculi, cerebellar cortex and various brainstem nuclei (Fig. 3a). This immunolabeling pattern was compatible with the expression pattern of synArfGEF mRNA in the rat brain described previously (Inaba *et al.* 2004). In control experiments, the primary antibody pre-absorbed with the antigen did not show any immunolabeling (Fig. 3b). In addition, both rabbit and guinea pig antibodies gave an identical labeling pattern (data not shown). Taken together, all these

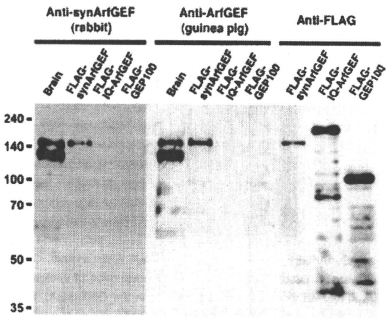

Fig. 2 Characterization of anti-synArfGEF antibodies by Western blot analysis. Lysates from mouse brain and COS-7 cells expressing FLAG-tagged synArfGEF, IQ-ArfGEF/BRAG1, or GEP100 were subjected to Western blot analysis with rabbit and guinea pig polyclonal antibodies against synArfGEF or anti-FLAG IgG.

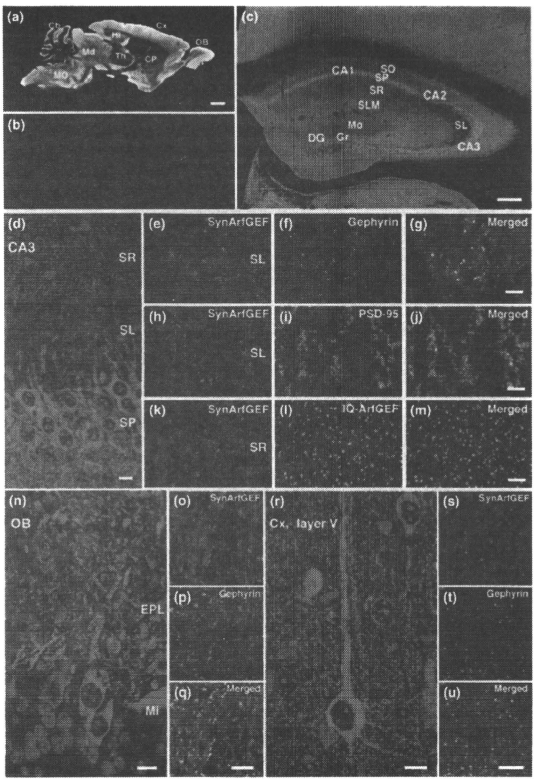

Fig. 3 Immunohistochemical localization of synArfGEF in the forebrain. (a, b) Sagittal sections from adult mouse brain were subjected to immunoperoxidase staining with the rabbit polyclonal anti-synArfGEF IgG (a) or antibody pre-absorbed with the antigen (10 μM) (b). Note the complete attenuation of immunolabeling by pre-incubation with the antigen. (c) Immunofluorescent localization of synArfGEF in the adult mouse hippocampus. (d–m) Immunofluorescent localization of synArfGEF in the hippocampal CA3 region. Coronal sections were immunostained for synArfGEF (e, h, k) and gephyrin (f), PSD-95 (i), or IQ-ArfGEF/BRAG1 (l). Note the colocalization of synArfGEF with gephyrin but not PSD-95 or IQ-ArfGEF. (n–q) Immunofluorescent localization of synArfGEF in the olfactory bulb. Note the colocalization of synArfGEF (o) and gephyrin (p) in the external plexiform layer (EPL). (r–u) Immunofluorescent localization of synArfGEF in the cerebral pyramidal neurons. Note the colocalization of synArfGEF (s) and gephyrin (t). Nuclei were counter-stained with 4′,6-diamidino-2-phenylindole dihydrochloride (DAPI) (blue) in panles d, n, and r. CA1-3, subfield CA1-3 of Ammon's horn; Cb, cerebellar cortex; CP, caudate putamen; Cx, cerebral cortex; DG, dentate gyrus; Gr, dentate granule cell layer; Hi, hippocampus; Md, midbrain; Mi, mitral cell layer; MO, medulla oblongata; Mo, molecular layer, OB, olfactory bulb; SL, stratum lucidum; SLM, stratum lacunosum-moleculare; SO, stratum oriens; SP, stratum pyramidale; SR, stratum radiatum; Th, thalamus. Scale bars, 1 mm (a); 200 μm (c); 10 μm (d, n, R); 5 μm (g, j, m, q, u).

findings suggest the immunolabeling observed with these antibodies is specific for synArfGEF.

In the hippocampus, synArfGEF immunoreactivity was widely distributed, with the highest level observed in the CA3 region (Fig. 3c). SynArfGEF labeling was observed diffusely in both neuronal somata and dendrites, but not in nuclei, of pyramidal cells. In addition to this diffuse cytoplasmic labeling, tiny puncta (< 1 μm in diameter) were distributed on the surface of the somata and dendrites (Fig. 3d), consistent with synaptic localization. To examine whether synArfGEF is associated with excitatory or inhibitory synapses, double immunofluorescence staining was performed with antibodies against synArfGEF and PSD-95, gephyrin or IQ-ArfGEF/BRAG1 (Fig. 3e–m). Extensive colocalization was observed between synArfGEF and gephyrin along somata and dendritic shafts (Fig. 3e–g), whereas synArfGEF puncta were rarely co-localized with PSD-95 or IQ-ArfGEF/BRAG1 (Fig. 3h–m).

In the olfactory bulb, synArfGEF immunoreactivity was distributed in the mitral cell, external plexiform, and glomerular layers (Fig. 3n). In mitral cells, somata and dendrites were heavily immunolabeled. Along their dendritic shafts in the external plexiform layer, synArfGEF labeling was distributed as puncta largely co-localized with gephyrin (Fig. 3o–q).

In the neocortex, synArfGEF immunoreactivity was distributed throughout the cortical layers. Pyramidal neurons in the layer V were intensely immunolabeled in their somatodendritic compartments without nuclear staining

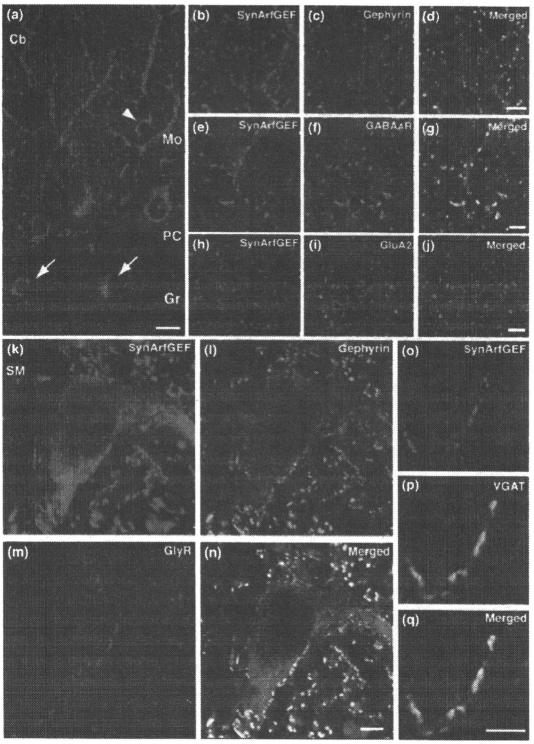

Fig. 4 Immunohistochemical localization of synArfGEF in the cerebellum and spinal cord. (a–j) Localization of synArfGEF in the cerebellar cortex (Cb). A sagittal section of the adult mouse cerebellar cortex (Cb) was immunostained for synArfGEF (b, e, h) and gephyrin (c), $GABA_AR$ α1 subunit (f), or GluA2 subunit (i). Note that immunolabeling of synArfGEF in the cell bodies of Purkinje cells, basket cells (arrowhead), stellate cells and Golgi cells (arrows) as well as dendrites of Purkinje cells in the molecular layer (Mo). Also note the colocalization of synArfGEF with gephyrin and $GABA_AR$ α1 subunit but not GluA2 subunit in the molecular layer. Gr, granular layer; PC, Purkinje cell layer. (k–q) Localization of synArfGEF in spinal motoneurons (SM). Coronal sections of the spinal cord were immunostained for synArfGEF (k), gephyrin (l) and glycine receptor α subunit (m) or with synArfGEF (o) and VGAT (p). Note the colocalization of synArfGEF, gephyrin and glycine receptor α subunit along the cell body/dendritic shafts and the close apposition of synArfGEF to VGAT. Scale bar, 20 μm (a); 5 μm (d, g, j, n, q).

(Fig. 3r). At high magnification, synArfGEF was found in fine puncta along the somata and dendrites, which were largely co-localized with gephyrin (Fig. 3s–u).

In the cerebellar cortex, synArfGEF immunoreactivity was observed in the somata and dendritic shafts of Purkinje cells, and the somata of basket cells and stellate cells in the molecular layer, and the somata of Golgi cells in the granular layer (Fig. 4a). However, the somata of granule cells were devoid of immunolabeling for synArfGEF. At high magnification, tiny immunoreactive puncta were found to be distributed along Purkinje cell dendrites and co-localized well with gephyrin (Fig. 4b–d) and $GABA_AR$ α1 subunit (Fig. 4e–g) without overlapping with α-amino-3-hydroxy-5-methyl-4-isoxazolepropionate receptor GluA2 subunit (Fig. 4h–j).

In the spinal cord, synArfGEF immunoreactivity was distributed in the gray matter. In particular, the somata and dendrites of ventral motoneurons were heavily immunolabeled (Fig. 4k). The immunoreactive puncta along the somata and dendritic shafts were largely co-localized with both glycine receptors and gephyrin (Fig. 4k–n). Immunoreactive puncta were also closely apposed to VGAT labeling, forming merged color at the interface (Fig. 4o–q). These confocal microscopic results suggest that synArfGEF is preferentially distributed at inhibitory synapses throughout the central nervous system.

To determine the precise synaptic localization, we performed pre-embedding immunogold electron microscopy in the external plexiform layer of the olfactory bulb (Fig. 5a), the molecular layer of the cerebellar cortex (Fig. 5b), and spinal motoneurons (Fig. 5c). Immunogold particles for synArfGEF accumulated on or beneath the post-synaptic membrane of symmetric synapses formed on dendritic shafts

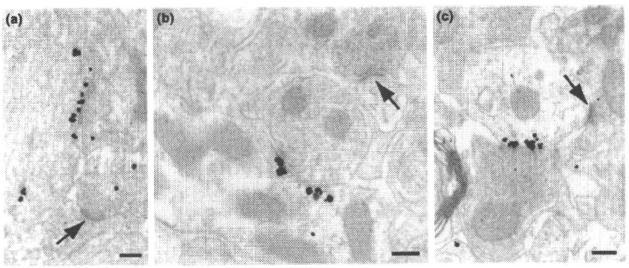

Fig. 5 Subcellular localization of synArfGEF by immunoelectron microscopy using the silver-enhanced immunogold method. Note the accumulation of immunogold particles for synArfGEF at post-synaptic specializations of symmetric synapses of the dendritic shafts of an olfactory mitral cell in the external plexiform layer (a), a Purkinje cell in the molecular layer (b), and a spinal motoneuron (c). Note the absence of immunolabeling at asymmetric synapses (arrows). Scale bars, 200 nm.

and cell bodies. By contrast, no significant immunogold particles were observed at asymmetric synapses on olfactory mitral cells (Fig. 5a), cerebellar Purkinje cells (Fig. 5b), or spinal motoneurons (Fig. 5c). These findings confirm that synArfGEF localizes exclusively at post-synaptic specializations of inhibitory synapses.

Interaction of synArfGEF with utrophin/dystrophin

To identify interacting proteins with synArfGEF, we performed yeast two-hybrid screening of a mouse brain cDNA library, using the C-terminal 73 amino acids of synArfGEF as bait. We isolated two independent cDNA clones (#5 and #57) encoding utrophin, a large cytoskeletal protein with high structural similarity to dystrophin (Fig. 6a). Both clones encoded an overlapping C-terminal region (amino acids 2698–3429) containing a partial 20th spectrin repeat, the WW and Zn^{2+} finger motifs, and two coiled-coil domains. As dystrophin was shown to localize at inhibitory synapses and to regulate the clustering of selected $GABA_AR$ subtypes (Knuesel *et al.* 1999), we further examined whether the corresponding C-terminal region of dystrophin (amino acids 2937–3685) could interact with the C-terminus of synArfGEF. Indeed, yeast expressing dystrophin 2937–3685 and synArfGEF 1122–1194 exhibited significant β-galactosidase activity and the ability to grow without histidine and uracil (Fig. 6b), indicating a robust protein-protein interaction. Next, we determined the region of utrophin responsible for the interaction with synArfGEF using two-hybrid assays with synArfGEF bait and various truncated mutants of utrophin as shown in Fig 6a. Yeast expressing synArfGEF and utrophin fragments 2691–3429, 2691–3111 and 2691–3058 exhibited detectable β-galactosidase activity, although the prototrophy for histidine and uracil was markedly disturbed in yeast expressing utrophin 2691–3111 and 2691–3058 (Fig. 6b). The interaction was not detected when utrophin 2691–3058 was further truncated (amino acids 2810–3058, 2691–2843, or 2810–2843) or the WW motif was deleted (utrophin fragments 2843–3429, 3061–3429, and 3249–3429) (Fig. 6a). These findings suggest that the minimal region of utrophin required for the interaction corresponds to amino acids 2691–3058.

The synArfGEF-utrophin interaction was also independently verified using pull down assays. Consistently, GST-utrophin 2691–3429, 2691–3058 and GST-dystrophin 2937–3685 were capable of efficient pull down of full-length FLAG-synArfGEF from transfected COS-7 cell lysates, whereas neither GST-utrophin 2691–2843 nor GST alone was capable of mediating this interaction (Fig. 6c). The synArfGEF-utrophin interaction was retained even when the salt concentration in the washing buffer was raised to 300 mM, although the interaction between GST-utrophin 2691–3058 and synArfGEF was decreased (Fig. 6c). Furthermore, GST-utrophin 2691–3429 and GST-dystrophin 2937–3685, but not GST alone, efficiently pulled down endogenous synArfGEF from brain extracts (Fig. 6d).

The C-terminal 73 amino acids of synArfGEF used as bait contain a proline-rich sequence and type I PDZ-binding motif. The proline-rich domain is followed by a tyrosine residue (sequence PPPPY), which forms a known motif for binding to WW domains – the PY motif (Chen and Sudol 1995; Rentschler *et al.* 1999) (Fig. 7a). As the minimal region of utrophin required for robust interactions with synArfGEF contains a WW motif, we examined whether this PY motif mediated the synArfGEF–utrophin interaction. Activation of reporter genes was observed when yeast was co-transformed with utrophin 2653–3429 and synArfGEF 1122–1194, ΔC3, 1122–1172, or 1141–1194, all of which contained the PY motif, although the β-galactosidase activity was dramatically reduced in the yeast transformed with

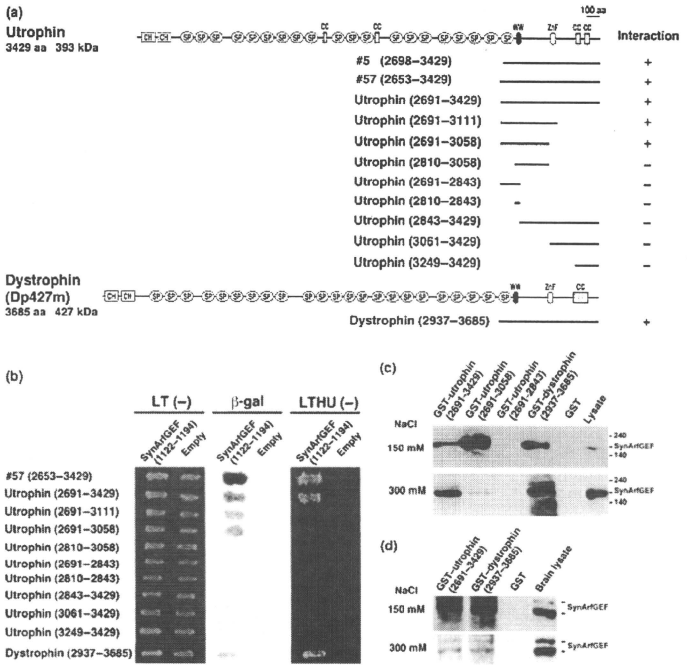

Fig. 6 Interaction of synArfGEF with utrophin/dystrophin. (a) Schematic representation of the domain structures of utrophin and dystrophin and the protein fragments used in the yeast two-hybrid assays. (b) Two-hybrid assays. The yeast strain MaV203 was transformed with the indicated combinations of constructs and plated onto synthetic complete medium lacking leucine and tryptophan: LT(–), or leucine, tryptophan, histidine and uracil: LTHU(–). Interactions were assessed by β-galactosidase activity (β-gal) and prototrophy for histidine and uracil. Note the interaction of synArfGEF with utrophin fragments 2653–3429, 2691–3429, 2691–3111, 2691–3058, and dystrophin fragment 2937–3685. (c, d) Pull down assays. Lysates from COS-7 cells transfected with pCAGGS-FLAG-synArfGEF (c) and mouse brains (d) were subjected to pull down assays with the indicated GST fusion proteins that were conjugated with glutathione-Sepharose 4B. The precipitates were washed with the lysis buffer containing 150 or 300 mM NaCl and subjected to Western blot analysis with anti-FLAG IgG (c) or anti-synArfGEF IgG (d).

utrophin 2653–3429 and synArfGEF 1122–1172 (Fig. 7b). The substitution of proline and tyrosine residues in the PY motif to alanine residues (PPPPY → PPAPA) disrupted the interaction between synArfGEF and utrophin (Fig. 7a and b), suggesting that the PY motif in synArfGEF is critical for this interaction.

To examine whether synArfGEF and utrophin/dystrophin co-localize at synapses, cultured hippocampal neurons were prepared from rat embryos, maintained for 22 days and immunostained with antibodies against synArfGEF and dystrophin or utrophin. Dendritic synArfGEF puncta showed extensive colocalization with dystrophin (Fig. 8b–d). By contrast, anti-utrophin did not immunolabel hippocampal neurons (data not shown). Furthermore, synArfGEF-immunoreactive puncta were also associated with $GABA_AR$ α1 subunit and VGAT but not with PSD-95 (Fig. 8e–m). Taken together, these findings suggest that synArfGEF and dystrophin form a complex at inhibitory synapses of hippocampal neurons *in vivo*, mediated by PY-motif and WW domain interactions.

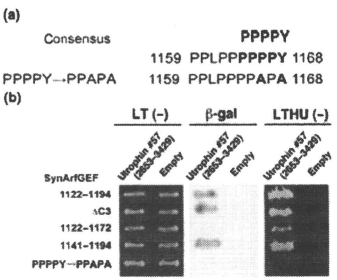

Fig. 7 Interaction of synArfGEF with utrophin via a PPPPY motif. (a) Sequence alignment of the consensus PPPPY motif required for binding to WW domains, proline-rich sequence of the C-terminal region of synArfGEF and the mutant (PPPPY → PPAPA). (b) Two-hybrid assays. The yeast strain MaV203 was transformed with the indicated combinations of constructs and plated onto synthetic complete medium lacking leucine and tryptophan: LT(−) or leucine, tryptophan, histidine and uracil: LTHU(−). Interactions were assessed by β-galactosidase activity (β-gal) and the ability to grow on LTHU(−) medium. Note the disruption of the interaction with utrophin by the mutation in a PPPPY motif (PPPPY → PPAPA).

Interaction of synArfGEF with S-SCAM/MAGI-2

In addition to utrophin, we also isolated several independent clones encoding the membrane-associated guanylate kinase with inverted orientation (MAGI) family, which contains six PDZ domains, two WW domains and one guanylate kinase domain and comprises of three members, MAGI-1, S-SCAM (also called MAGI-2), and MAGI-3. S-SCAM was previously shown to localize at inhibitory synapses and to act as a molecular bridge between the neurexin-neuroligin complex and the DGC via direct interactions with two adhesion molecules at inhibitory synapses, neuroligin-2 and β-dystroglycan (Sumita *et al.* 2007). We therefore examined whether synArfGEF could interact with S-SCAM using pull down assays (Fig. 9a). GST-synArfGEF 1122–1194 efficiently pulled down full-length S-SCAM from lysates of transfected COS-7 cells. We further determined which region of S-SCAM was responsible for this interaction using various truncated S-SCAM mutants as shown in Fig. 9a. GST-synArfGEF 1122–1194 could efficiently pull down S-SCAM 295–578 containing two WW domains and the PDZ1 domain, while it could not pull down S-SCAM 1–301 or 573–1277. Although the binding efficiency was drastically reduced, S-SCAM 425–578 containing only PDZ1 domain retained the ability to bind to GST-synArfGEF 1122–1194 (Fig. 9a), indicating that PDZ1 domain is the minimal requirement for the interaction with synArfGEF.

To examine whether synArfGEF co-localizes with S-SCAM at synapses, we performed double immunofluorescent staining of the cerebellar cortex (Fig. 9b). In the molecular layer, both synArfGEF and S-SCAM were distributed in puncta, although S-SCAM puncta were slightly larger in size. The anti-synArfGEF IgG labeled 43% of S-SCAM puncta (n = 202), whereas the anti-S-SCAM IgG labeled 26% of synArfGEF puncta (n = 335). These findings suggest that synArfGEF partially co-localizes with S-SCAM in the cerebellar molecular layer.

Finally, we performed co-immunoprecipiation experiments from brain lysates to examine whether synArfGEF forms a proteins complex with dystrophin and S-SCAM *in vivo*. The anti-synArfGEF IgG, but not normal rabbit IgG, efficiently immunoprecipitated S-SCAM from the deoxycholate-solubilized P2 fraction (Fig. 9c). Although we failed to detect dystrophin or utrophin in the immunoprecipitates (data not shown), the anti-synArfGEF IgG clearly immunoprecipitated

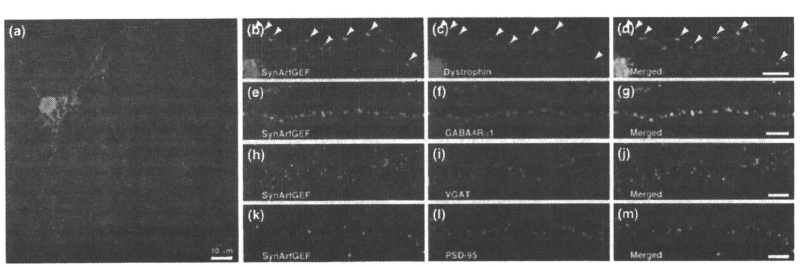

Fig. 8 Colocalization of synArfGEF and dystrophin at inhibitory synapses of cultured hippocampal neurons. Cultured hippocampal neurons at 22 DIV were immunostained with anti-synArfGEF (a, b, e, h, k) and anti-dystrophin (c), $GABA_AR$ α1 subunit (f), VGAT (i) or PSD-95 (l) antibodies. Note the close association of synArfGEF with dystrophin, $GABA_AR$ α1 and VGAT but not with PSD-95. Arrowheads in high-magnification views (b–d) show the colocalization of endogenous synArfGEF and dystrophin along dendrites. Scale bars, 10 μm (a); 5 μm (d, g, j, m).

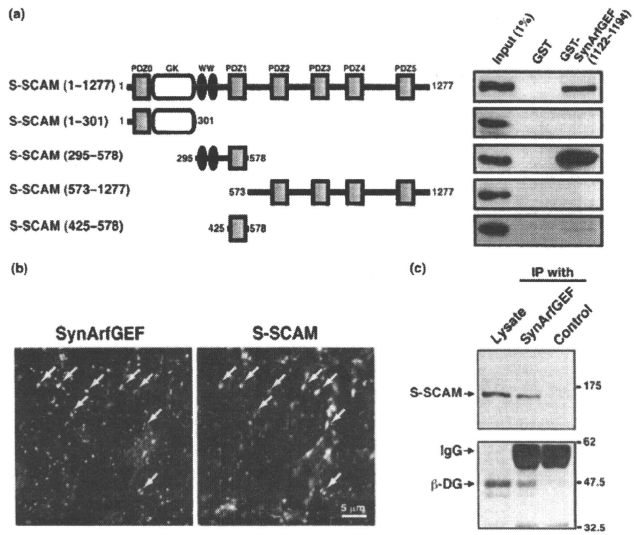

Fig. 9 Interaction of synArfGEF with S-SCAM. (a) Pull down assays. COS-7 cells were transfected with the S-SCAM constructs shown in the left panel and subjected to pull down assays with GST-synArfGEF 1122–1194. Note the interaction of GST-synArfGEF 1122–1194 with S-SCAM fragments 1–1277, 295–578, and 425–578. (b) Immunofluorescent staining of the cerebellar molecular layer, showing the partial colocalization of synArfGEF and S-SCAM (arrows). (c) Co-immunoprecipitation assays. Deoxycholate-solubilized P2 fractions were immunoprecipitated with anti-synArfGEF IgG or normal rabbit IgG and subjected to Western blot analysis with antibodies against S-SCAM and β-dystroglycan (β-DG). Note the co-immunoprecipitation of S-SCAM and β-dystroglycan with synArfGEF from brain lysates.

β-dystroglycan from the deoxycholate-solubilized P2 fraction (Fig. 9c). Taken together, these results suggest that synArfGEF is likely to be present in the DGC and associate with S-SCAM at inhibitory synapses.

Discussion

The BRAG/IQSEC family is composed of three members, IQ-ArfGEF/BRAG1/IQSEC2, GEP100/BRAG2/IQSEC1, and synArfGEF/BRAG3/IQSEC3, all of which share characteristic domain organization containing an N-terminal IQ-like motif, a central Sec7 domain and pleckstrin homology domain (Table 1). GEP100/BRAG2/IQSEC1, a prototypical member of this family, was shown to activate Arf6 *in vitro* and *in vivo* (Someya *et al.* 2001; Morishige *et al.* 2008). IQ-ArfGEF/BRAG1/IQSEC2 was subsequently shown to activate Arf6 using pull down assays with GST-GGA1 (Sakagami *et al.* 2008). In this study, we have shown that synArfGEF/BRAG3/IQSEC3 also functions as a GEF for Arf6 *in vivo* by using pull down and transferrin incorporation assays. However, we were unable to conclusively demonstrate the GEF activity of synArfGEF toward Arf1, because co-transfection of synArfGEF and Arf1 increased total Arf1 in the lysate to the same extent as GTP-Arf1 pulled down by GST-GGA1. By contrast, Hattori *et al.* (2007) have previously shown that KIAA1110, encoding a human homologue of synArfGEF, exhibits GEF activity toward Arf1 but not Arf6 using an Arf pull down assay with the same GST-GGA1. The reasons for this discrepancy are unknown at present. However, as KIAA1110 is a partial 770 amino acid protein corresponding to amino acids 439–1194 of rat synArfGEF, the complete structure of synArfGEF may be required for GEF activity toward Arf6.

The PSD of excitatory synapses is known to contain a diverse array of GEFs and GTPase-activating proteins (GAPs) for small GTPases: Ras-GAP (synGAP) (Chen *et al.* 1998), Arf-GEFs (BRAG1, BRAG2b) (Murphy *et al.* 2006; Dosemeci *et al.* 2007; Sakagami *et al.* 2008), Arf-GAPs (GIT1 and PIKE-L) (Peng *et al.* 2004), Rac-GEF (Kalirin) (Penzes *et al.* 2000), Rap-GEF (cAMP-GEFII/Epac2) (Peng

Table 1 BRAG/IQSEC family proteins and interactors and key roles in synaptic function

Gene symbol and chromosomol location	Other names	GTPase specificity	Interacting proteins/proposed biological function	References
IQSEC1 3p25.2 (human) *Iqsec1* 6qDI (mouse)	GEP 100 BRAG2 IQSEC1 KIAA0763 p100	Arf1, Arf5, **Arf6**	• BRAG2 activating of Arf6 regulates endocytosis and recycling of β1 integrins • Alpha-catenin binding to ArfGEP100 activates Arf6, resulting in E-cadherin recycling and actin re-modelling • BRAG2 interacts with α-amino-3-hydroxy-5-methyl-4-isoxazolepropionate (AMPA) receptor subunit GluA2 and activates Arf6, thereby internalizing synaptic AMPA receptors upon LTD induction	Dunphy *et al.* (2006) Hiroi *et al.* (2006) Scholz *et al.* (2010)
IQSEC2 Xp11.22 (human) *Iqsec2* XqF3 (mouse)	IQ-ArfGEF BRAG1 IQSEC2 K1AA0522	Arf1, **Arf6**	• IQ-ArfGEF selectively activates Arf6 and forms a complex with NDMA receptors via interactions with PSD95 at excitatory synapses • IQ-ArfGEF interacts with insulin receptor tyrosine kinase substrate p53 (IRSp53) at excitatory PSDs via its C-terminal proline-rich sequence • IQ-ArfGEF mRNA is dendritically localized • IQ-ArfGEF/BRAG1 localizes as retinal synaptic ribbons and forms a protein complex with RIBEYE • Missense mutations in *IQSEC2* cause non-syndromic X-linked intellectual disability	Murphy *et al.* (2006) Dosemeci *et al.* (2007) Sanda *et al.* (2009) Katsumata *et al.* (2009) Shoubridge *et al.* (2010)
IQSEC3 l2pl3.33 (human) *Iqsec3* 6qF1 (mouse)	SynArfGEF BRAG3 IQSEC3 KIAA1110	Arf1, **Arf6**	• SynArfGEF is able to interact with PSD-95, SAP97 and Homer/VesII/PSD-Zip45 via a C-terminal PDZ-binding motif • SynArfGEF mRNA is dendritically localized • SynArfGEF selectively activates Arf6 and interacts with scaffolding proteins utrophin/dystrophin and S-SCAM/MAGI-2 at inhibitory synapses	Inaba *et al.* (2004) Hattori *et al.* (2007) This study

et al. 2004), and Rap-GAP (SPAR) (Pak *et al.* 2001). These regulatory proteins for small GTPases are proposed to modulate synaptic transmission by regulating the formation and maintenance of dendritic spines and synapses through the actin cytoskeleton reorganization (Penzes *et al.* 2001; Zhang *et al.* 2003, 2005; Vazquez *et al.* 2004; Woolfrey *et al.* 2009). Among the BRAG family, IQ-ArfGEF/BRAG1/IQSEC2 was shown to localize at the PSD of excitatory synapses and form a protein complex with NMDA-type glutamate receptors, possibly via an interaction with PSD-95 (Murphy *et al.* 2006; Dosemeci *et al.* 2007; Sakagami *et al.* 2008) and insulin receptor tyrosine kinase substrate of 53 kDa (IRSp53) (Sanda *et al.* 2009) (Table 1). Mutations in *IQSEC2* have recently been reported in patients with non-syndromic X chromosome-linked intellectual disability (Shoubridge *et al.* 2010). Interestingly, mutations in three of four separate families with non-syndromic X chromosome-linked intellectual disability lead to amino acid substitutions in the Sec7 domain and consequent reduction of the GEF activity toward Arf6, suggesting the functional significance of IQSEC2-Arf6 pathway in neuronal morphology or synaptic plasticity (Shoubridge *et al.* 2010). In sharp contrast, we show that synArfGEF localizes preferentially at post-synaptic specializations of inhibitory synapses. This major finding was confirmed by several independent lines of immunohistochemical evidence. To our knowledge, the only known regulator of small GTPases found at inhibitory post-synaptic specializations is collybistin, a GEF for Cdc42, which was identified as an interacting protein for gephyrin by yeast two-hybrid screening (Kins *et al.* 2000). Thus, synArfGEF is listed as the second known regulator of GTPase that shows preferential localization at post-synaptic specializations of inhibitory synapses.

What are the potential roles of synArfGEF at inhibitory synapses? The Arf family comprises six structurally related members that regulate membrane trafficking and the actin cytoskeleton (D'Souza-Schorey and Chavrier 2006). Of the six Arf members, Arf6 is localized at the plasma membrane and endosomes, and regulates the endosome-plasma membrane traffic and remodeling of the actin cytoskeleton at the cell surface. At synapses, the submembrane cytoskeleton is known to regulate the number and dynamics of neurotransmitter receptors on the post-synaptic membrane, thereby modulating synaptic efficacy. At inhibitory synapses, both

actin and microtubules have been shown to regulate the lateral diffusion and stabilization of glycine receptors and gephyrin (Charrier *et al.* 2006). In addition, gephyrin interacts with various regulatory proteins for the cytoskeleton, including polymerized tubulin (Kirsch *et al.* 1991), profilin (Mammoto *et al.* 1998) and mammalian enabled/vasodilator stimulated phosphoprotein (Giesemann *et al.* 2003). In turn, gephyrin depends on both actin and microtubules for synaptic apposition and scaffold formation (Kirsch and Betz 1995). It is therefore possible that synArfGEF may initiate local remodeling of the synaptic submembrane actin cytoskeleton through the activation of Arf6, thereby modulating the lateral diffusion and stabilization of neurotransmitter receptors and gephyrin at inhibitory synapses.

Another noteworthy finding is that synArfGEF interacts with utrophin/dystrophin and S-SCAM via a PY motif and PDZ-binding motif in the C-terminal region, respectively. The ability of synArfGEF to bind utrophin/dystrophin was verified by both yeast two-hybrid and pull down assays. Although we failed to detect dystrophin or utrophin in co-immunoprecipitation assays, β-dystroglycan and S-SCAM were immunoprecipitated from brain lysates by the anti-synArfGEF IgG. Consistent with previous findings demonstrating that dystrophin and S-SCAM are localized to inhibitory synapses (Knuesel *et al.* 1999; Sumita *et al.* 2007), immunostaining showed the colocalization of synArfGEF with dystrophin and S-SCAM. However, the anti-utrophin antibody raised in this study did not result in any immunolabeling in the cultured hippocampal neurons. This is consistent with previous findings suggesting that utrophin transcripts are predominantly expressed in endothelial cells of blood vessels rather than in neurons (Knuesel *et al.* 2000). Hence, it is likely that S-SCAM and dystrophin, but not utrophin, are physiological binding partners for synArfGEF. At inhibitory synapses, dystrophin forms the DGC with α- and β-dystroglycan, syntrophin, and α- and β-dystrobrevin. Intriguingly, S-SCAM was shown to interact directly with two inhibitory post-synaptic components, β-dystroglycan and neuroligin-2 (Sumita *et al.* 2007). Thus, the interaction of synArfGEF with dystrophin and S-SCAM enables synArfGEF to activate Arf6 in the proximity of the DGC and neuroligin-2 at inhibitory post-synaptic specializations. Mdx mice lacking a long form of dystrophin exhibit a marked reduction in the clustering of $GABA_A$Rs containing the α2 subunit but retain gephyrin clustering in the cerebellar cortex, suggesting a dystrophin-dependent and gephyrin-independent mechanism for the clustering of selected $GABA_A$R subtypes. In the future, it will be of particular interest to examine the possibility that synArfGEF is involved in the dystrophin-dependent clustering of $GABA_A$Rs through Arf6-dependent actin cytoskeleton remodeling.

Finally, it should be noted that the interaction of synArfGEF with dystrophin and S-SCAM cannot account for the specific mechanism for the targeting of synArfGEF to inhibitory synapses, because dystrophin and S-SCAM are only present at a subset of inhibitory synapses and S-SCAM is present at both excitatory and inhibitory synapses (Knuesel *et al.* 1999; Levi *et al.* 2002; Sumita *et al.* 2007). Therefore, additional factors are required for specific targeting of synArfGEF to inhibitory synapses.

In conclusion, we have demonstrated that synArfGEF activates Arf6 and localizes preferentially at inhibitory post-synaptic specializations, forming a protein complex with the DGC and S-SCAM using distinct binding motifs. These findings link Arf6 signaling pathways to inhibitory synapses and suggest that synArfGEF may influence dynamic processes affecting the synaptic localization of inhibitory $GABA_A$ and glycine receptors.

Acknowledgements

We thank Dr Kazuhisa Nakayama (Kyoto University Graduate School of Pharmaceutical Sciences) for the expression vectors for HA-tagged Arf1, Arf6 and GST-GGA1-GAT fusion protein, Dr Masanobu Satake (Tohoku University) for FLAG-tagged Arf6 in pCAGGS-neo, Dr James M. Ervasti (University of Minnesota) for FLAG-utrophin in pFASTBac1, Dr Jun-ichi Miyazaki (Osaka University Medical School) for pCAGGS vector. This work was supported by Grants-in-Aid for Scientific Research to H.S. (#2165049 and #22300114) from the Ministry of Education, Science, Sports, Culture, and Technology of Japan and grants from Kitasato University (All Kitasato Project Study and Integrative Research Program #2009-A01).

Supporting information

Additional Supporting information may be found in the online version of this article:

Figure S1. The specificity of antibodies against gephyrin, S-SCAM, and utrophin.

Figure S2. Characterization of anti-synArfGEF antibodies by immunostaining.

Table S1. Primer combinations used in this study.

As a service to our authors and readers, this journal provides supporting information supplied by the authors. Such materials are peer-reviewed and may be re-organized for online delivery, but are not copy-edited or typeset. Technical support issues arising from supporting information (other than missing files) should be addressed to the authors.

References

Brunig I., Suter A., Knuesel I., Luscher B. and Fritschy J. M. (2002) GABAergic terminals are required for postsynaptic clustering of dystrophin but not of GABA(A) receptors and gephyrin. *J. Neurosci.* **22**, 4805–4813.

Charrier C., Ehrensperger M. V., Dahan M., Levi S. and Triller A. (2006) Cytoskeleton regulation of glycine receptor number at synapses and diffusion in the plasma membrane. *J. Neurosci.* **26**, 8502–8511.

Chen H. I. and Sudol M. (1995) The WW domain of Yes-associated protein binds a proline-rich ligand that differs from the consensus established for Src homology 3-binding modules. *Proc. Natl Acad. Sci. USA* **92**, 7819–7823.

Chen H. J., Rojas-Soto M., Oguni A. and Kennedy M. B. (1998) A synaptic Ras-GTPase activating protein (p135 SynGAP) inhibited by CaM kinase II. *Neuron* **20**, 895–904.

Choi S., Ko J., Lee J. R., Lee H. W., Kim K., Chung H. S., Kim H. and Kim E. (2006) ARF6 and EFA6A regulate the development and maintenance of dendritic spines. *J. Neurosci.* **26**, 4811–4819.

Claing A. (2004) Regulation of G protein-coupled receptor endocytosis by ARF6 GTP-binding proteins. *Biochem. Cell Biol.* **82**, 610–617.

Cox R., Mason-Gamer R. J., Jackson C. L. and Segev N. (2004) Phylogenetic analysis of Sec7-domain-containing Arf nucleotide exchangers. *Mol. Biol. Cell* **15**, 1487–1505.

Delaney K. A., Murph M. M., Brown L. M. and Radhakrishna H. (2002) Transfer of M2 muscarinic acetylcholine receptors to clathrin-derived early endosomes following clathrin-independent endocytosis. *J. Biol. Chem.* **277**, 33439–33446.

Dosemeci A., Makusky A. J., Jankowska-Stephens E., Yang X., Slotta D. J. and Markey S. P. (2007) Composition of the synaptic PSD-95 complex. *Mol. Cell Proteomics* **6**, 1749–1760.

D'Souza-Schorey C. and Chavrier P. (2006) ARF proteins: roles in membrane traffic and beyond. *Nat. Rev. Mol. Cell Biol.* **7**, 347–358.

D'Souza-Schorey C., Li G., Colombo M. I. and Stahl P. D. (1995) A regulatory role for ARF6 in receptor-mediated endocytosis. *Science* **267**, 1175–1178.

Dunphy J. L., Moravec R., Ly K., Lasell T. K., Melancon P. and Casanova J. E. (2006) The Arf6 GEF GEP100/BRAG2 regulates cell adhesion by controlling endocytosis of beta1 integrins. *Curr. Biol.* **16**, 315–320.

Essrich C., Lorez M., Benson J. A., Fritschy J. M. and Luscher B. (1998) Postsynaptic clustering of major GABAA receptor subtypes requires the gamma 2 subunit and gephyrin. *Nat. Neurosci.* **1**, 563–571.

Feng G., Tintrup H., Kirsch J., Nichol M. C., Kuhse J., Betz H. and Sanes J. R. (1998) Dual requirement for gephyrin in glycine receptor clustering and molybdoenzyme activity. *Science* **282**, 1321–1324.

Fritschy J. M., Harvey R. J. and Schwarz G. (2008) Gephyrin: where do we stand, where do we go? *Trends Neurosci.* **31**, 257–264.

Fukaya M. and Watanabe M. (2000) Improved immunohistochemical detection of postsynaptically located PSD-95/SAP90 protein family by protease section pretreatment: a study in the adult mouse brain. *J. Comp. Neurol.* **426**, 572–586.

Fukudome Y., Ohno-Shosaku T., Matsui M. *et al.* (2004) Two distinct classes of muscarinic action on hippocampal inhibitory synapses: M2-mediated direct suppression and M1/M3-mediated indirect suppression through endocannabinoid signalling. *Eur. J. Neurosci.* **19**, 2682–2692.

Giesemann T., Schwarz G., Nawrotzki R. *et al.* (2003) Complex formation between the postsynaptic scaffolding protein gephyrin, profilin, and Mena: a possible link to the microfilament system. *J. Neurosci.* **23**, 8330–8339.

Grady R. M., Wozniak D. F., Ohlemiller K. K. and Sanes J. R. (2006) Cerebellar synaptic defects and abnormal motor behavior in mice lacking alpha- and beta-dystrobrevin. *J. Neurosci.* **26**, 2841–2851.

Gray E. G. (1959) Axo-somatic and axo-dendritic synapses of the cerebral cortex: an electron microscope study. *J. Anat.* **93**, 420–433.

Harvey K., Duguid I. C., Alldred M. J. *et al.* (2004) The GDP-GTP exchange factor collybistin: an essential determinant of neuronal gephyrin clustering. *J. Neurosci.* **24**, 5816–5826.

Hattori Y., Ohta S., Hamada K., Yamada-Okabe H., Kanemura Y., Matsuzaki Y., Okano H., Kawakami Y. and Toda M. (2007) Identification of a neuron-specific human gene, KIAA1110, that is a guanine nucleotide exchange factor for ARF1. *Biochem. Biophys. Res. Commun.* **364**, 737–742.

Hernandez-Deviez D. J., Casanova J. E. and Wilson J. M. (2002) Regulation of dendritic development by the ARF exchange factor ARNO. *Nat. Neurosci.* **5**, 623–624.

Hernandez-Deviez D. J., Roth M. G., Casanova J. E. and Wilson J. M. (2004) ARNO and ARF6 regulate axonal elongation and branching through downstream activation of phosphatidylinositol 4-phosphate 5-kinase alpha. *Mol. Biol. Cell* **15**, 111–120.

Hiroi T., Someya A., Thompson W., Moss J. and Vaughan M. (2006) GEP100/BRAG2: activator of ADP-ribosylation factor 6 for regulation of cell adhesion and actin cytoskeleton via E-cadherin and alpha-catenin. *Proc. Natl. Acad. Sci. USA* **103**, 10672–10677.

Hosaka M., Toda K., Takatsu H., Torii S., Murakami K. and Nakayama K. (1996) Structure and intracellular localization of mouse ADP-ribosylation factors type 1 to type 6 (ARF1–ARF6). *J. Biochem. (Tokyo)* **120**, 813–819.

Houndolo T., Boulay P. L. and Claing A. (2005) G protein-coupled receptor endocytosis in ADP-ribosylation factor 6-depleted cells. *J. Biol. Chem.* **280**, 5598–5604.

Inaba Y., Tian Q. B., Okano A. *et al.* (2004) Brain-specific potential guanine nucleotide exchange factor for Arf, synArfGEF (Po), is localized to postsynaptic density. *J. Neurochem.* **89**, 1347–1357.

Katsumata O., Ohara N., Tamaki H., Niimura T., Naganuma H., Watanabe M. and Sakagami H. (2009) IQ-ArfGEF/BRAG1 is associated with synaptic ribbons in the mouse retina. *Eur. J. Neurosci.* **30**, 1509–1516.

Kins S., Betz H. and Kirsch J. (2000) Collybistin, a newly identified brain-specific GEF, induces submembrane clustering of gephyrin. *Nat. Neurosci.* **3**, 22–29.

Kirsch J. and Betz H. (1995) The postsynaptic localization of the glycine receptor-associated protein gephyrin is regulated by the cytoskeleton. *J. Neurosci.* **15**, 4148–4156.

Kirsch J., Langosch D., Prior P., Littauer U. Z., Schmitt B. and Betz H. (1991) The 93-kDa glycine receptor-associated protein binds to tubulin. *J. Biol. Chem.* **266**, 22242–22245.

Kirsch J., Wolters I., Triller A. and Betz H. (1993) Gephyrin antisense oligonucleotides prevent glycine receptor clustering in spinal neurons. *Nature* **366**, 745–748.

Kneussel M. and Betz H. (2000) Receptors, gephyrin and gephyrin-associated proteins: novel insights into the assembly of inhibitory postsynaptic membrane specializations. *J. Physiol.* **525**(Pt 1), 1–9.

Knuesel I., Mastrocola M., Zuellig R. A., Bornhauser B., Schaub M. C. and Fritschy J. M. (1999) Short communication: altered synaptic clustering of GABAA receptors in mice lacking dystrophin (mdx mice). *Eur. J. Neurosci.* **11**, 4457–4462.

Knuesel I., Bornhauser B. C., Zuellig R. A., Heller F., Schaub M. C. and Fritschy J. M. (2000) Differential expression of utrophin and dystrophin in CNS neurons: an in situ hybridization and immunohistochemical study. *J. Comp. Neurol.* **422**, 594–611.

Krauss M., Kinuta M., Wenk M. R., De Camilli P., Takei K. and Haucke V. (2003) ARF6 stimulates clathrin/AP-2 recruitment to synaptic membranes by activating phosphatidylinositol phosphate kinase type Igamma. *J. Cell Biol.* **162**, 113–124.

Levi S., Grady R. M., Henry M. D., Campbell K. P., Sanes J. R. and Craig A. M. (2002) Dystroglycan is selectively associated with inhibitory GABAergic synapses but is dispensable for their differentiation. *J. Neurosci.* **22**, 4274–4285.

Mammoto A., Sasaki T., Asakura T., Hotta I., Imamura H., Takahashi K., Matsuura Y., Shirao T. and Takai Y. (1998) Interactions of drebrin

and gephyrin with profilin. *Biochem. Biophys. Res. Commun.* **243**, 86–89.

Morishige M., Hashimoto S., Ogawa E. *et al.* (2008) GEP100 links epidermal growth factor receptor signalling to Arf6 activation to induce breast cancer invasion. *Nat. Cell Biol.* **10**, 85–92.

Murphy J. A., Jensen O. N. and Walikonis R. S. (2006) BRAG1, a Sec7 domain-containing protein, is a component of the postsynaptic density of excitatory synapses. *Brain Res.* **1120**, 35–45.

Niwa H., Yamamura K. and Miyazaki J. (1991) Efficient selection for high-expression transfectants with a novel eukaryotic vector. *Gene* **108**, 193–199.

Pak D. T., Yang S., Rudolph-Correia S., Kim E. and Sheng M. (2001) Regulation of dendritic spine morphology by SPAR, a PSD-95-associated RapGAP. *Neuron* **31**, 289–303.

Papadopoulos T., Korte M., Eulenburg V. *et al.* (2007) Impaired GABAergic transmission and altered hippocampal synaptic plasticity in collybistin-deficient mice. *EMBO J.* **26**, 3888–3899.

Peng J., Kim M. J., Cheng D., Duong D. M., Gygi S. P. and Sheng M. (2004) Semiquantitative proteomic analysis of rat forebrain postsynaptic density fractions by mass spectrometry. *J. Biol. Chem.* **279**, 21003–21011.

Penzes P., Johnson R. C., Alam M. R., Kambampati V., Mains R. E. and Eipper B. A. (2000) An isoform of kalirin, a brain-specific GDP/GTP exchange factor, is enriched in the postsynaptic density fraction. *J. Biol. Chem.* **275**, 6395–6403.

Penzes P., Johnson R. C., Sattler R., Zhang X., Huganir R. L., Kambampati V., Mains R. E. and Eipper B. A. (2001) The neuronal Rho-GEF Kalirin-7 interacts with PDZ domain-containing proteins and regulates dendritic morphogenesis. *Neuron* **29**, 229–242.

Pfeiffer F., Graham D. and Betz H. (1982) Purification by affinity chromatography of the glycine receptor of rat spinal cord. *J. Biol. Chem.* **257**, 9389–9393.

Poulopoulos A., Aramuni G., Meyer G. *et al.* (2009) Neuroligin 2 drives postsynaptic assembly at perisomatic inhibitory synapses through gephyrin and collybistin. *Neuron* **63**, 628–642.

Rentschler S., Linn H., Deininger K., Bedford M. T., Espanel X. and Sudol M. (1999) The WW domain of dystrophin requires EF-hands region to interact with beta-dystroglycan. *Biol. Chem.* **380**, 431–442.

Sakagami H., Kamata A., Fukunaga K. and Kondo H. (2005) Functional assay of EFA6A, a guanine nucleotide exchange factor for ADP-ribosylation factor 6 (ARF6), in dendritic formation of hippocampal neurons. *Methods Enzymol.* **404**, 232–242.

Sakagami H., Suzuki H., Kamata A., Owada Y., Fukunaga K., Mayanagi H. and Kondo H. (2006) Distinct spatiotemporal expression of EFA6D, a guanine nucleotide exchange factor for ARF6, among the EFA6 family in mouse brain. *Brain Res.* **1093**, 1–11.

Sakagami H., Honnma T., Sukegawa J., Owada Y., Yanagisawa T. and Kondo H. (2007) Somatodendritic localization of EFA6A, a guanine nucleotide exchange factor for ADP-ribosylation factor 6, and its possible interaction with alpha-actinin in dendritic spines. *Eur. J. Neurosci.* **25**, 618–628.

Sakagami H., Sanda M., Fukaya M. *et al.* (2008) IQ-ArfGEF/BRAG1 is a guanine nucleotide exchange factor for Arf6 that interacts with PSD-95 at postsynaptic density of excitatory synapses. *Neurosci. Res.* **60**, 199–212.

Sanda M., Kamata A., Katsumata O., Fukunaga K., Watanabe M., Kondo H. and Sakagami H. (2009) The postsynaptic density protein, IQ-ArfGEF/BRAG1, can interact with IRSp53 through its proline-rich sequence. *Brain Res.* **1251**, 7–15.

Scannevin R. H. and Huganir R. L. (2000) Postsynaptic organization and regulation of excitatory synapses. *Nat. Rev. Neurosci.* **1**, 133–141.

Scholz R., Berberich S., Rathgeber L., Kolleker A., Kohr G. and Kornau H. C. (2010) AMPA receptor signaling through BRAG2 and Arf6 critical for long-term synaptic depression. *Neuron* **66**, 768–780.

Shinotsuka C., Yoshida Y., Kawamoto K., Takatsu H. and Nakayama K. (2002) Overexpression of an ADP-ribosylation factor-guanine nucleotide exchange factor, BIG2, uncouples brefeldin A-induced adaptor protein-1 coat dissociation and membrane tubulation. *J. Biol. Chem.* **277**, 9468–9473.

Shoubridge C., Tarpey P. S., Abidi F. *et al.* (2010) Mutations in the guanine nucleotide exchange factor gene IQSEC2 cause nonsyndromic intellectual disability. *Nat. Genet.* **42**, 486–488.

Someya A., Sata M., Takeda K., Pacheco-Rodriguez G., Ferrans V. J., Moss J. and Vaughan M. (2001) ARF-GEP(100), a guanine nucleotide-exchange protein for ADP-ribosylation factor 6. *Proc. Natl Acad. Sci. USA* **98**, 2413–2418.

Sumita K., Sato Y., Iida J., Kawata A., Hamano M., Hirabayashi S., Ohno K., Peles E. and Hata Y. (2007) Synaptic scaffolding molecule (S-SCAM) membrane-associated guanylate kinase with inverted organization (MAGI)-2 is associated with cell adhesion molecules at inhibitory synapses in rat hippocampal neurons. *J. Neurochem.* **100**, 154–166.

Takatsu H., Yoshino K., Toda K. and Nakayama K. (2002) GGA proteins associate with Golgi membranes through interaction between their GGAH domains and ADP-ribosylation factors. *Biochem. J.* **365**, 369–378.

Tanabe K., Torii T., Natsume W., Braesch-Andersen S., Watanabe T. and Satake M. (2005) A novel GTPase-activating protein for ARF6 directly interacts with clathrin and regulates clathrin-dependent endocytosis. *Mol. Biol. Cell* **16**, 1617–1628.

Vazquez L. E., Chen H. J., Sokolova I., Knuesel I. and Kennedy M. B. (2004) SynGAP regulates spine formation. *J. Neurosci.* **24**, 8862–8872.

Vitale N., Chasserot-Golaz S., Bailly Y., Morinaga N., Frohman M. A. and Bader M. F. (2002) Calcium-regulated exocytosis of dense-core vesicles requires the activation of ADP-ribosylation factor (ARF)6 by ARF nucleotide binding site opener at the plasma membrane. *J. Cell Biol.* **159**, 79–89.

Woolfrey K. M., Srivastava D. P., Photowala H. *et al.* (2009) Epac2 induces synapse remodeling and depression and its disease-associated forms alter spines. *Nat. Neurosci.* **12**, 1275–1284.

Yamazaki M., Fukaya M., Hashimoto K. *et al.* (2010) TARPs gamma-2 and gamma-7 are essential for AMPA receptor expression in the cerebellum. *Eur. J. Neurosci.* **31**, 2204–2220.

Zhang H., Webb D. J., Asmussen H. and Horwitz A. F. (2003) Synapse formation is regulated by the signaling adaptor GIT1. *J. Cell Biol.* **161**, 131–142.

Zhang H., Webb D. J., Asmussen H., Niu S. and Horwitz A. F. (2005) A GIT1/PIX/Rac/PAK signaling module regulates spine morphogenesis and synapse formation through MLC. *J. Neurosci.* **25**, 3379–3388.

Crosstalk between Glucocorticoid Receptor and Nutritional Sensor mTOR in Skeletal Muscle

Noriaki Shimizu,[1,10] Noritada Yoshikawa,[1,2,10] Naoki Ito,[3,4] Takako Maruyama,[1] Yuko Suzuki,[3] Sin-ichi Takeda,[3] Jun Nakae,[5] Yusuke Tagata,[9] Shinobu Nishitani,[9] Kenji Takehana,[9] Motoaki Sano,[6] Keiichi Fukuda,[6] Makoto Suematsu,[7,8] Chikao Morimoto,[1,2] and Hirotoshi Tanaka[1,2,*]

[1]Division of Clinical Immunology, Advanced Clinical Research Center
[2]Department of Rheumatology and Allergy, Research Hospital
Institute of Medical Science, University of Tokyo, Tokyo 108-8639, Japan
[3]Department of Molecular Therapy, National Institute of Neuroscience, National Center of Neurology and Psychiatry, Kodaira 187-8502, Japan
[4]Department of Biological Information, Tokyo Institute of Technology, Yokohama 226-8501, Japan
[5]Frontier Medicine on Metabolic Syndrome, Division of Endocrinology, Metabolism and Nephrology, Department of Internal Medicine
[6]Cardiology Division, Department of Internal Medicine
[7]Department of Biochemistry
[8]JST ERATO, Suematsu Gas Biology Project
Keio University School of Medicine, Tokyo 160-8582, Japan
[9]Ajinomoto Pharmaceuticals Co., Ltd., Kawasaki 210-8681, Japan
[10]These authors contributed equally to this work
*Correspondence: hirotnk@ims.u-tokyo.ac.jp
DOI 10.1016/j.cmet.2011.01.001

SUMMARY

Maintenance of skeletal muscle mass relies on the dynamic balance between anabolic and catabolic processes and is important for motility, systemic energy homeostasis, and viability. We identified direct target genes of the glucocorticoid receptor (GR) in skeletal muscle, i.e., REDD1 and KLF15. As well as REDD1, KLF15 inhibits mTOR activity, but via a distinct mechanism involving BCAT2 gene activation. Moreover, KLF15 upregulates the expression of the E3 ubiquitin ligases atrogin-1 and MuRF1 genes and negatively modulates myofiber size. Thus, GR is a liaison involving a variety of downstream molecular cascades toward muscle atrophy. Notably, mTOR activation inhibits GR transcription function and efficiently counteracts the catabolic processes provoked by glucocorticoids. This mutually exclusive crosstalk between GR and mTOR, a highly coordinated interaction between the catabolic hormone signal and the anabolic machinery, may be a rational mechanism for fine-tuning of muscle volume and a potential therapeutic target for muscle wasting.

INTRODUCTION

Muscle comprises ~40% of body mass and contributes not only to the structure and movement of the body but also to nutrient storage and supply (Matthews, 1999). In adult mammals, skeletal muscle hypertrophy/atrophy is characterized by an increase/decrease in the size (as opposed to the number) of individual myofibers, respectively. The control of muscle mass is believed to be determined by a dynamic balance between anabolic and catabolic processes (Hoffman and Nader, 2004). Mammalian target of rapamycin (mTOR) is a crucial component of the anabolic machinery for protein synthesis. mTOR consists of two complexes: mTORC1, which includes Raptor, signals to S6K and 4E-BP1, controls protein synthesis, and is rapamycin sensitive; and mTORC2, which includes Rictor, signals to Akt, and is rapamycin insensitive. mTORC1 integrates four major signals: growth factors, energy status, oxygen, and amino acids, especially branched-chain amino acids (BCAAs). Prototypically, insulin/IGF-1 activates mTOR via the PI3K-Akt pathway (Sengupta et al., 2010). It is currently considered that mTORC1, and not mTORC2, is essential for the maintenance of muscle mass and function (Bentzinger et al., 2008; Risson et al., 2009). Protein degradation in skeletal muscle cells is essentially mediated by the activity of two conserved pathways: the ubiquitin-proteasomal pathway and the autophagic/lysosomal pathway (Sandri, 2008). The ubiquitin-proteasomal pathway is responsible for the turnover of the majority of soluble and myofibrillar muscle proteins. The activity of this pathway is markedly increased in atrophying muscle due to the transcriptional activation of a set of E3 ligase-encoding genes, e.g., atrogin-1 and MuRF1 (Glass, 2003; Sandri et al., 2004). Autophagy also plays an important role in the degradation of skeletal muscle, and is indicated to be a consequence of an ordered transcriptional program involving a battery of genes, e.g., LC3 and Bnip3 (Mizushima et al., 2008). These positive and negative pathways are balanced in a highly coordinated manner for the determination of myofiber size and total muscle volume; however, distortion of this balance with a relative increase in degradation results in the generalized decrease of myofiber size and muscle atrophy (Hoffman and Nader, 2004). Pioneering studies demonstrated that muscle atrophy is a result of active processes that are transcriptionally controlled through the expression of a particular gene set; the forkhead box O (FoxO) transcription factors are

common components of a number of atrophy models and act as critical liaison molecules for protein degradation and autophagy via the transcriptional regulation of, for example, atrogin-1, MuRF1, LC3, and Bnip3 (Mammucari et al., 2007; Sandri et al., 2004; Stitt et al., 2004; Zhao et al., 2007). In clear contrast, it is evident that each disease has proper signaling pathways to FoxOs and that other components of the cellular machinery often participate in the progression of atrophy (Moresi et al., 2010; Suzuki et al., 2007). Therefore, for the development of therapies against muscle atrophy, it should be addressed how the transcriptional program triggered by a particular atrophy pathway is orchestrated and how the balance of muscle protein synthesis and degradation is distorted in each disease.

Adrenal glucocorticoids produce their actions via a signal pathway involving the ubiquitously expressed glucocorticoid receptor (GR), a prototypic member of the nuclear receptor superfamily, which acts as a ligand-dependent transcription factor. Upon binding glucocorticoids, GR translocates into the nucleus and binds to the glucocorticoid response element (GRE) in the promoters of target genes. The binding of liganded receptors to target DNA is followed by the recruitment of mediators and coactivators to the proximity of GRE, resulting in the recruitment of RNA polymerase II (RNAPII) to nearby transcription start sites and the activation of transcription (Evans, 2005; Meijsing et al., 2009). In skeletal muscle, glucocorticoids elicit a variety of biological actions in the metabolism of glucose, lipids, and proteins and contribute to metabolic homeostasis (Munck et al., 1984). On the other hand, the prolonged oversecretion or exogenous administration of glucocorticoid gives rise to undesirable effects including muscle atrophy (Munck et al., 1984). Although many studies addressed the mechanism of glucocorticoid-induced muscle atrophy, how the glucocorticoid-GR system generates the functional coupling between metabolic regulation and volume adjustment in skeletal muscle remains unsolved. Of note, many pathological conditions characterized by muscle atrophy, e.g., sepsis, cachexia, starvation, metabolic acidosis, and severe insulinopenia, are associated with an increase in circulating glucocorticoid levels. Adrenalectomy or treatment with the GR antagonist RU486 attenuates muscle atrophy in sepsis, cachexia, starvation, and severe insulinopenia (Menconi et al., 2007; Schakman et al., 2008). Moreover, endogenous glucocorticoids were shown to be essential for muscle atrophy in acute diabetic rodents (Hu et al., 2009). Together, understanding the glucocorticoid-mediated regulation of metabolism-volume coupling in muscle is increasingly important for the management of not only muscle atrophy but also these wasting/metabolic disorders.

Typically, glucocorticoid-induced muscle atrophy is characterized by fast-twitch type II glycolytic muscle fiber loss with reduced or no impact on type I fibers. The mechanism of such fiber specificity is yet unknown. Previous reports suggested that the glucocorticoid-GR system has antianabolic and catabolic effects and promotes degradation via the induction of a set of genes including atrogin-1, MuRF1, and myostatin (Menconi et al., 2007; Schakman et al., 2008). Although the involvement of FoxO transcription factors is reported in the gene regulation of atrogin-1 and MuRF1 under the presence of excess glucocorticoids (Sandri et al., 2004; Stitt et al., 2004), the biochemical role of GR in the transcriptional regulation of muscle tissue has not yet been determined. Therefore, we investigated how GR-mediated gene expression coordinately modulates antianabolic and catabolic actions to understand the functional coupling of metabolism and volume regulation in muscle.

In the present study, we identified REDD1 and KLF15 genes as direct targets of GR. REDD1 is known to be induced by various stressors, including glucocorticoid, and to inhibit mTOR activity via the sequestration of 14-3-3 and the increase of TSC1/2 activity (Wang et al., 2006; DeYoung et al., 2008). We clearly identified the functional GRE via the promoter analysis of REDD1 gene. On the other hand, KLF15 is a recently discovered transcription factor that is involved in several metabolic processes in skeletal muscle; e.g., KLF15 transcriptionally upregulates the gene expression of branched-chain aminotransferase 2 (BCAT2), a mitochondrial enzyme catalyzing the first reaction in the catabolism of BCAA to accelerate BCAA degradation and alanine production in skeletal muscle (Gray et al., 2007). Moreover, phenotypic analysis of cardiac-specific KLF15 knockout mice revealed marked left ventricular hypertrophy, indicating the negative regulatory role of KLF15 on muscle mass (Fisch et al., 2007). We here demonstrated that KLF15 participates in muscle catabolism via the transcriptional regulation of atrogin-1 and MuRF1. Moreover, KLF15 affects mTOR through BCAA degradation and negatively modulates myofiber size. mTOR activation inhibits GR-mediated transcription by suppressing GR recruitment onto target genes, strongly suggesting a mutually exclusive crosstalk between mTOR and GR. Pharmacological activation of mTOR with BCAA attenuated GR-mediated gene expression, leading to the substantial restoration of muscle in glucocorticoid-treated rats. We, therefore, indicate the critical importance of the interaction of GR and mTOR in the regulation of metabolism-volume coupling in skeletal muscle.

RESULTS

REDD1 and KLF15 Are Target Genes of GR in Skeletal Muscle

GR levels were relatively high in type II-rich gastrocnemius and tibialis anterior muscles compared to type I-rich soleus muscle in rats (Figure 1A). Figure 1B illustrates the comparison of the effects of a 3 hr treatment with dexamethasone (DEX) on mRNA expression of various genes between the gastrocnemius and soleus muscles. Hormonal induction of mRNA expression of REDD1, atrogin-1, MuRF1, KLF15, FoxO1, FoxO3, and myostatin, as well as the well-known GR target gene FKBP5 (Yoshikawa et al., 2009), was observed in both muscles, but to a lesser extent in the soleus muscle. Among the genes induced by DEX at 3 hr (Figure 1B), the promoter regions of MuRF1 (Waddell et al., 2008) and myostatin (Ma et al., 2001), but not atrogin-1 (Sandri et al., 2004), contain functional GREs. In addition, REDD1 and KLF15 were also considered as candidates of GR target genes (see the Supplemental Information available online).

Concerning KLF15, we showed, in gastrocnemius muscle and L6 myotubes but not in liver, that KLF15 mRNA and protein expression was induced in a GR-dependent manner (Figure 2A). The promoter region spanning from −4676 to +116 of KLF15 gene was not responsive to DEX; however, the activity of the region spanning −2108 to +1331 was induced by DEX, and